Mon. Not. R. Astron. Soc. **291,** 252–272 (1997)

Rotation, activity and lithium in NGC 6475

David J. James[1]★† and Robin D. Jeffries[2]★

[1]*School of Physics and Space Research, University of Birmingham, Edgbaston, Birmingham B15 2TT*
[2]*Department of Physics, Keele University, Keele, Staffordshire ST5 5BG*

Accepted 1997 June 27. Received 1997 May 23; in original form 1997 February 3

ABSTRACT

Radial and rotational velocities, chromospheric activity and lithium abundances are presented for an X-ray-selected sample of stars in the young (220 Myr) open cluster NGC 6475. Low-mass members of the cluster have been identified on the basis of photometric and spectroscopic criteria. The observations show that the rapid spin-down seen amongst solar-type stars in the Pleiades is incomplete at 220 Myr, as there are F, G and K stars in NGC 6475 with $v \sin i > 10$ km s^{-1}. Peak rotation rates for G stars are 12–14 km s^{-1} and are robust to uncertain inclination angles, because the magnetic activity of these stars is less than the saturation value observed for fast rotators ($v \sin i > 15$ km s^{-1}) in the Pleiades. Two mid-K stars are found with $v \sin i \sim 25$ km s^{-1} and with saturated magnetic activity levels, indicating that spin-down time-scales are mass dependent, increasing from ~ 20 Myr for early-G stars to > 75 Myr for mid-K stars. We have compared our rotation data, for the most rapidly rotating G and K stars in NGC 6475 and in young open clusters, with published rotational evolution models incorporating magnetic dynamo saturation at high rotation rates ($> \Omega_{sat}$). Models with interior angular momentum transport are unable to simultaneously fit the rapidly rotating stars of the α Per, Pleiades and NGC 6475 clusters. Likely solutions are a plausible increase in the age of the Pleiades to 100 Myr, the incorporation of centrifugal wind driving in the angular momentum loss treatment, or ad hoc differences in initial conditions. If an increase in the age of the Pleiades is assumed, we find that a mass dependent Ω_{sat} is required, such that dynamo saturation occurs for G and K stars at a Rossby number of ~ 0.4. This value is incompatible with the faster saturation thresholds inferred from coronal X-rays, but Ω_{sat} can be increased if solid body rotation is enforced or centrifugal wind driving is included. Comparisons with such models are favourable for G stars but less so for K stars. This may result from neglecting the evolving moment of inertia at early ages.

All the cool stars exhibit Li I 6708-Å absorption features. When compared to Li in the Pleiades and Hyades, it is evident that the G and K stars in the Hyades have experienced substantial Li depletion whilst on the main sequence, between 220 and 600 Myr, and probably at earlier times on the main sequence as well. There is marginal scatter of about 0.1 dex in the Li abundances of G and early K stars, possibly increasing to 1.0 dex in a few cooler objects. The data are insufficient to allow us to decide whether there is a mechanism by which to eliminate the scatter in Li abundances of the Pleiades K stars before they reach the Hyades age, or whether the difference reflects different cluster initial conditions. Interpretation is complicated by the X-ray selection bias, favouring the observation of the more rapidly rotating, Li-rich stars. Metallicity may also play a role, but our spectral

★E-mail: djj@st-and.ac.uk (DJJ); rdj@astro.keele.ac.uk (RDJ)
†Present address: School of Physics and Astronomy, University of St. Andrews, North Haugh, St. Andrews, Fife KY16 9SS.

synthesis estimate of [Fe/H] = +0.110±0.034 is comparable to the Pleiades and Hyades values.

Key words: stars: abundances – stars: activity – stars: late-type – stars: rotation – open clusters and associations: individual: NGC 6475 – X-rays: stars.

1 INTRODUCTION

Rotation and convection are believed to be the dominant processes governing the evolution of magnetic activity and lithium depletion in late-type stars. Investigation of these processes has largely been achieved through observations of coeval stars in open clusters of different ages. An empirical understanding of how observational properties such as rotation rate, X-ray emission and lithium abundance vary with time, leads to constraints on angular momentum loss (AML) mechanisms, dynamo models and non-standard features of stellar evolutionary models such as rotational mixing or microscopic diffusion.

AML is generally thought to occur via a decoupling of the ionized stellar wind from the stellar magnetic field at some distance from the surface (Schatzmann 1962; Weber & Davis 1967). As a result, convective late-type stars, in which an internal dynamo is thought to generate and amplify magnetic fields, spin-down as they age. The evolution of rotation and magnetic activity in solar-type stars was quantified approximately with a $t^{-1/2}$ decay relation by Wilson (1963, 1966), Kraft (1967) and Skumanich (1972). The dependence of magnetic activity on age arises implicitly because of the well-known rotation–activity correlation (Noyes et al. 1984).

Projected equatorial rotation velocities ($v \sin i$) and some rotation periods have been measured for late-type dwarfs in the α Persei open cluster (age 50 Myr – Stauffer, Hartmann & Jones 1989; Prosser 1992), the Pleiades (age 70 Myr – Stauffer & Hartmann 1987; Soderblom et al. 1993a, hereafter S93) and the Hyades (age 600 Myr – Radick et al. 1987; Stauffer, Hartmann & Latham 1987). While the results for the slowest rotators largely agree with a $t^{-1/2}$ decay law, there are ultra-fast rotators (UFRs – $v \sin i > 20$ km s^{-1}) in these clusters, which cannot be explained in the same way (see Stauffer 1991 for a review). In the α Per cluster about 50 per cent of the G stars are UFRs, reducing to 20 per cent in the Pleiades. For the K and M stars the fractions of UFRs in the two clusters are similar. By contrast, there are no UFR G or early/mid-K stars in the Hyades, where rotation rates have converged to an almost unique function of mass, but there are a few UFR M stars. This implies that the spin-down of late-type stars is mass dependent, with a time-scale of roughly 20 Myr for G stars and anywhere between 50 and 1000 Myr for K and M stars.

The spread in rotation rates as late-type stars reach the zero-age main sequence (ZAMS) can be explained in terms of magnetic coupling to an accretion disc during the pre-main sequence (PMS) phase. The disc acts as a rotostat, until it is disrupted or disappears and then the decreasing moment of inertia as the star approaches the ZAMS leads to spin-up. The stars which had the shortest disc lifetimes became the UFRs (see for example Collier Cameron, Campbell & Quaintrell 1995). Two alternative explanations have been advanced for the mass-dependent spin-down of UFRs. The first assumes that the radiative core and convective envelope can rotationally decouple (Endal & Sofia 1981; Stauffer et al. 1987; Li & Collier Cameron 1993). Decoupling is attractive because convection zone depth and its fractional contribution to the moment of inertia increases with decreasing mass and only the envelope is spun down by the magnetized stellar wind. Observations have revealed significant rotation in some horizontal branch stars indicative of angular momentum (AM) re-emergence from the interior (Peterson 1985; Pinsonneault, Deliyannis & De Marque 1991). At present, the time-scale, mechanisms and mass-dependency of core-envelope decoupling are poorly understood and the role of a poloidal magnetic field threading the radiative and convective zones may prove crucial (Charbonneau & MacGregor 1993). An alternative view is that the magnetic field strengths saturate in the most rapidly rotating stars. The evidence for this comes mainly from the observations of saturation in magnetic activity indicators such as X-ray emission (Stauffer et al. 1994). Models incorporating threshold rotation speeds for B-field saturation, both with and without core-envelope decoupling, have been developed by a number of authors (Collier Cameron & Li 1994, hereafter CC94; MacGregor & Charbonneau 1994; Barnes & Sofia 1996, hereafter BS96). Models with no decoupling also require B-field saturation to match observational data, but at much higher angular velocities (15–45 $\Omega_\odot$) than models with decoupling (5–10 $\Omega_\odot$). The saturation of chromospheric and coronal magnetic activity indicators (Vilhu 1984; Stauffer et al. 1994) favours the latter scenario, but O'Dell et al. (1995) have argued that photospheric starspot coverage continues to increase at much higher rotation speeds. A requirement of both types of model is that the saturation threshold is mass dependent. Observationally this is an open question, but it is plausible when one considers the convective properties of late-type stars. The efficiency of the dynamo is related to both the rotation period, P, and the convective turnover time, τ_c, through the Rossby number ($R_o = P/\tau_c$). B-field strength and activity increase with inverse Rossby number and τ_c is larger in lower-mass stars. If AML saturates at a given Rossby number, this will be equivalent to a smaller saturation rotation speed in lower-mass stars.

The fragile element lithium is destroyed in stellar interiors by ^{7}Li$(p,\alpha)^4$He reactions above $\approx 2.5 \times 10^6$ K. Convective mixing in late-type stars during PMS evolution is sufficiently deep to cause Li depletion, which increases as a function of decreasing mass (D'Antona & Mazzitelli 1984; Proffitt & Michaud 1989). On the main sequence (MS), solar-metallicity standard stellar evolution models predict little or no Li depletion in late-type stars with $T_{\rm eff} \geq 5300$ K

during their MS lifetimes. Furthermore, MS Li depletion is predicted to be a unique function of mass, age and composition (see Pinsonneault 1994 for a review of the standard model). Such predictions are at variance with open cluster observations of the neutral lithium resonance doublet at 6708 Å (Li I). Late-F and G Hyads exhibit substantial MS Li depletion from the levels of their almost undepleted Pleiades counterparts. K dwarfs in the Pleiades do show PMS Li depletion, but there is a scatter of up to 2 orders of magnitude, which cannot be explained with standard models. A correlation between Li abundance and rotation has been noted in both clusters, in the sense that rapid rotators have suffered less Li depletion (Soderblom et al. 1993b; Balachandran, Lambert & Stauffer 1988, 1996). There is also evidence for MS depletion in K stars, because K-dwarf Hyads have no detectable Li (Thorburn et al. 1993; Soderblom et al. 1995). The time-scales for this MS depletion are poorly defined because of the large age gap between the Pleiades and Hyades and the fact that the Pleiades K stars have not yet reached the ZAMS. Soderblom et al. (1993c) have presented Li abundances in the UMa moving Group, which has an approximate age of 300 Myr. These observations may show that MS depletion occurs between ages of 70 and 600 Myr at a decelerating rate. The interpretation is confused by problematic identification of members of the kinematic group and metallicity differences between the Hyades and the UMa group (Chaboyer, DeMarque & Pinsonneault 1995).

In this paper, we present X-ray observations and intermediate to high-resolution spectroscopic observations of an X-ray selected sample of late-type stars in NGC 6475. This young, nearby, open cluster (age 220 Myr, distance $\sim$250 pc – Meynet et al. 1993), also known as Ptolemy's cluster, is a well-populated southern hemisphere object in the Scorpius constellation situated about 4° south of the Galactic plane (RA $17^{h}53^{m}$, Dec. $-34°52.8'$, J2000). The cluster is at a diagnostically important age between the well-studied Pleiades and Hyades. The key questions that we wish to address through observations of this cluster are the following. (1) What are the spin-down time-scales for late-G and K stars? (2) Can rotation evolution models match the rotation rates of stars between the ages of the Pleiades and Hyades, and what constraints are placed upon core-envelope decoupling and saturation rotation rates? (3) What is the time dependence of Li depletion whilst stars are on the main sequence?

Our sample consists of optical counterparts to *ROSAT* X-ray sources which, on the basis of their photometry, have been suggested as cluster members by Prosser et al. (1995, hereafter P95), Prosser (private communication) and Prosser, Randich & Stauffer (1996). Spectroscopy has allowed confirmation of cluster membership and/or binarity through radial velocity measurements, and we have also obtained projected equatorial velocities ($v \sin i$), chromospheric activity indices and Li abundances.

The paper is structured as follows: in Section 2 we describe our observations and data analyses. In Section 3 we present the results of the X-ray and spectroscopic observations, while a discussion of the data and a comparison to other young open clusters is presented in Section 4. Rotation rates of the most rapidly rotating G and K stars in the α Per, Pleiades, NGC 6475 and Hyades clusters are compared with some current solid-body and core-envelope decoupling AML evolutionary models in Section 5. We conclude and summarize our arguments in Section 6.

2 OBSERVATIONS AND DATA ANALYSES

2.1 *ROSAT* data

The X-ray observations used in this paper come from P95 and an independent 27 ks *ROSAT* observation of NGC 6475 obtained between 1993 March 22 and 25. The position sensitive proportional counter (PSPC; see Briel & Pfeffermann 1986) was used at the focal plane, with a pointing position of RA $= 17^{h}53^{m}09.6^{s}$ and Dec. $= -34°52'48.0''$, J2000.0. A summary of the X-ray data reduction is outlined here, while a comprehensive treatment of all the NGC 6475 X-ray data is deferred to another paper. The observations were binned into spatial images, with a pixel size of 15 arcsec and using instrumental energy channels 11–41 and 52–201 (corresponding to approximate photon energies of $\sim$0.1–0.4 keV and $\sim$0.5–2.0 keV, referred to as the soft and hard wavebands). Times of high particle background were excluded from the analyses, amounting to 9 per cent of the total exposure time.

Count rates and source positions were determined using a maximum likelihood point source searching (PSS) method, optimizing source and background strengths with respect to the Cash likelihood statistic (PSS is an algorithm incorporated into the ASTERIX software package, Allan 1992). PSS was performed on the soft and hard bands using a Cash statistic threshold of 4.5σ above the local background. Simulations have shown that this threshold results in less than one spurious source inside the central 20 arcmin radius PSPC field (Jeffries, Thurston & Pye 1997). Raw counts were corrected for the exposure time, dead-time, quantum efficiency variations and vignetting to give an on-axis count rate. Hard-band count rates were converted to X-ray fluxes (0.1–2.4 keV) assuming a PSPC conversion factor (CF) of 1 count $s^{-1} \equiv 1.8 \times 10^{-11}$ erg cm^{-2} s^{-1}. This CF was determined by fitting a two-component thermal model to a spectrum formed from the sum of several confirmed cluster sources. The two temperatures obtained were $T_1 = 0.52$ keV and $T_2 = 1.96$ keV (the emission measure ratio of these components has a range of 5–25, with a best-fitting value of 12) and a column density, N_H, of $10^{20.6}$ cm^{-2}. Using the interstellar absorption/reddening relationship given in Bohlin, Savage & Drake (1978), this hydrogen column is equivalent to a reddening, $E(B-V) = 0.06$, similar to the optically determined value obtained by Meynet, Mermilliod & Maeder (1993). Nine of the stars dealt with in this paper were detected in the X-ray observations described in P95, which were offset from our observation by 10 arcmin. For consistency, we use the PSPC count rates quoted by P95, but convert them to a flux using our derived CF. X-ray luminosities were calculated for all sources, assuming a common cluster distance of 250 pc.

2.2 Selection of spectroscopic targets

A sample of optical counterparts to PSPC X-ray sources in NGC 6475 has been constructed, in order to perform follow-up high-resolution spectroscopic observations. The

original target list consisted of bright ($V \lesssim 14$) stars inside the 30-arcsec PSPC error circles of X-ray detections. The positions of the stars were taken either from the Hubble Guide Star Catalogue (GSC, Version 1.1) or measured on a pneumatic X–Y measuring machine at the University of Birmingham, with respect to 30 SAO catalogue stars in the same field. UK Schmidt plate J663 was used, which was a 3600 s exposure taken on 1974 June 20. A six-coefficient transform gave positions with an rms error of about an arcsec, comparable with the GSC precision.

Field star contamination is problematic because the cluster lies in the Galactic plane ($b \sim -4°$), and up to 10–12 optical counterparts may be included in the 30-arcsec error circles. The high stellar density apparent on CCD frames and optical plates means that a significant fraction of apparent cluster members will still be field stars. At the time of our X-ray observations, few photometric and proper motion data were available for stars in the vicinity of NGC 6475. We obtained BVI_C photometry and Ca II H and K intermediate spectroscopy data at the South African Astronomical Observatory (SAAO) for a number of the brighter stars, from which we were able to assign photometric membership and detect evidence of chromospheric activity. The final high-resolution spectroscopic sample contained a combination of photometric cluster members, chromospherically active stars, and bright optical counterparts within PSPC error circles. In total, 66 and 15 stars were observed spectroscopically at high and intermediate resolution, respectively. In this paper, we report and discuss the observations of photometric candidates[1] inside PSPC X-ray error circles (see Section 3.1 for more detailed selection criteria), while the presentation and discussion of X-ray, spectroscopic and photometric data for cluster non-members is deferred to a forthcoming paper.

2.3 High-resolution spectroscopy

High-resolution spectra of the X-ray selected sample were obtained with echelle coudé spectrographs at the Mount Stromlo (MSO) 1.9-m telescope on 1994 June 22–23 and at the Anglo-Australian Observatory 3.9-m telescope (AAT) on 1993 July 30–31 and August 1, 1994 June 27–29 and 1996 February 9–11. The MSO observations were performed with a 79-line mm^{-1} grating, a 2048×2048 pixel Tektronix CCD and a 2-arcsec slit width, yielding a resolution of 0.15 Å at Hα. The AAT observations were performed using the UCLES spectrograph (Walker & Diego 1985), a 79-line mm^{-1} grating, 1024×1024 pixel Tektronix CCD and a 1.2-arcsec slit, which gave a resolution of 0.16 Å at Hα. The MSO and AAT spectra were reduced using the ECHOMOP software (Mills & Webb 1994) at the Birmingham Starlink node. The slit lengths were long enough to allow sky subtraction of the spectra. The signal-to-noise ratios (S/N) of the AAT spectra were in the range 10–50 per pixel at Hα, whereas the MSO spectra were poorer, with S/N $\sim$ 10–15 at Hα.

The spectra were used to obtain heliocentric radial velocities and $v \sin i$, using cross-correlation techniques (Tonry & Davis 1979). The spectral ranges used were $\lambda\lambda$5875–5955 Å for the MSO spectra and $\lambda\lambda$5671–5731 Å for the AAT spectra. These orders contained many metal absorption lines and little telluric contamination. Radial velocity zero-points were set by reference to spectra of several IAU radial velocity standard stars. For the AAT spectra these were HR 3748, 4786, 6970, 6468 and 5384, while for the MSO spectra HR 4786, 6468 and 6970 were used. HR 9032 was also observed at the AAT, but we chose not to use it during the analysis, since we calculate a radial velocity of $+15.7 \pm 0.4$ km s^{-1} whereas the standard value is $+13.8 \pm 0.4$ km s^{-1}, indicating possible variability. Cross-correlation of each standard star spectrum with those of the other radial velocity standards revealed that external errors on the standard system were about 0.2 km s^{-1}. Random errors arising from the poorer S/N of the target spectra, spectral-type mismatch between target and standard and the effects of broadening (see below), were determined by multiple simulations. Errors varied from 0.2 km s^{-1} for slowly rotating stars observed at the AAT, increasing to 2–3 km s^{-1} for targets rotating at $\geq$20 km s^{-1}. Similarly, the errors in the MSO radial velocities were estimated by simulation. Errors varied from 0.8 km s^{-1} for the slowest star, increasing to $\sim$2.5–4 km s^{-1} for the two UFRs observed. Radial velocities for JJ 39 (moderate S/N AAT observation of a UFR), and JJ 43, which is too hot to use cross-correlation methods (see Table 2, below), were calculated using the Doppler shift of their Hα lines. The accuracy of this method is estimated to be of order 5–8 km s^{-1}.

The full width at half maximum (FWHM) of the cross-correlation peaks obtained with slowly rotating inactive standard star spectra, of spectral types similar to the targets, were measured to provide $v \sin i$ measurements. The standard stars were chosen to have minimal activity in the chromospheric Ca II H and K lines, with rotation periods estimated from a correlation between rotation and chromospheric activity (Rutten 1987). The relationship between the FWHM of the cross-correlation peak and $v \sin i$ was calibrated by convolving the standard star spectra with limb-darkened ($\varepsilon = 0.6$) rotational broadening profiles (Gray 1992) and cross-correlating with the unbroadened templates. Random errors were calculated by multiple simulations, and are extremely sensitive to S/N and rotation, with variations of $\sim$1–3 and $\sim$2–10 km s^{-1} for the AAT and MSO targets, respectively. The minimum-activity standards used, their estimated rotation periods and spectral types are listed in Table 1.

Table 1. Data for the minimum-activity standard stars, taken from Rutten (1987).

Name	B–V	Spectral Type	Period (days)
HD 222368	0.51	F7 V	10.0
HD 187691	0.55	F8 V	15.0
HD 115617	0.71	G6 V	38.0
HD 149661	0.82	K2 V	21.3
HD 4628	0.88	K2 V	38.0
HD 16160	0.98	K3 V	45.0
HD 156026	1.16	K5 V	18.0

[1]To ensure consistency, all photometry in this paper is taken from P95, Prosser (private communication) and Prosser et al. (1996).

The AAT and MSO data both contain the Hα line, and the AAT spectra also contain an order which includes one of the Ca II infrared triplet (IRT) lines at 8542 Å. The IRT lines at 8498, 8542 and 8662 Å originate in the same higher levels as the Ca II H and K lines and have previously been used as chromospheric diagnostics (Linsky et al. 1979; Foing et al. 1989; S93). For each of these lines, an estimate of chromospheric activity has been made using a spectral subtraction technique. Spectra were rectified with low-order polynomials and the telluric features present in the Hα spectra were removed by comparison with a rapidly rotating B-star spectrum. Spectra of minimum-activity standard stars, of the nearest colour to the target star, were broadened, shifted to the radial velocity of each target and subtracted. The residual emission is taken as representative of the chromospheric contribution to the line.

The excess chromospheric Hα equivalent width (EW) was measured by integration of the residual emission. The Hα absorption feature of each target was fitted with a Gaussian. The limits of the EW integration were set at $\pm 2\sigma$ from the absorption centroid. The statistical errors on EW measurements have been calculated over the same 2σ limits. The same spectral subtraction procedure was also used to measure the 8542-Å IRT line.

The Li I 6708-Å EWs were measured using a similar technique. The same minimum-activity standard stars were used, which should be appropriate because they are slowly rotating, presumably quite old and can effectively be assumed to be completely Li depleted. The exception is HD 222368, for which a Li I 6708-Å EW of 26 mÅ has been reported (Favata, Micela & Sciortino 1996). An additive correction of +26 mÅ has been made to all target Li I EWs when the template used was HD 222368. A weak ($\sim$10-mÅ) Fe I line at 6707.44 Å lies close to the Li I doublet, which may lead to an overestimate of the lithium EW. An advantage of using a subtraction method is that, to first order, it accounts for blending with the Fe I line and other local molecular features, and permits a more accurate measure of the local continuum level under the effects of rotational broadening. As with the activity indices, a systematic error may be introduced if the temperature or metallicity of the template and target stars are significantly different. The blended lines are so weak that the statistical error in the EW measurements is more important.

2.4 Intermediate resolution spectroscopy

Intermediate resolution spectra of several NGC 6475 photometric members were obtained on 1993 June 1, 6 and 7 with the 1.9-m telescope at the SAAO, equipped with the UNIT spectrograph and the Reticon Photon Counting System. An 830-line mm^{-1} grating was used at the Cassegrain focal station with a 1.5-arcsec slit width to give a resolution of $\sim$1 Å and a wavelength coverage of 3600–4250 Å. Spectra were flat-fielded with long quartz lamp exposures and corrected for atmospheric extinction using data from Spencer-Jones (1980). Wavelength calibration was achieved by reference to Argon arc lamp spectra. Heliocentric radial velocities were obtained using the cross-correlation technique. Radial velocity zero-points were set by reference to multiple measurements of two radial velocity standard star spectra, HD 203638 and HR 6468. The error associated with these measurements is estimated to be about 5 km s^{-1} for slowly rotating targets, and increases with increasing rotation rate and decreasing S/N.

3 RESULTS

3.1 Identification of cluster members

The intent of this paper is to present X-ray, spectroscopic and photometric data for a sample of cluster members which are optical counterparts to PSPC X-ray sources. Cluster membership is hard to judge decisively. We have used both photometric and spectroscopic data as follows. A cluster member must have photometry consistent with the colour–magnitude diagram (CMD) for NGC 6475. Practically, we set a limit of between 0.5 mag below and 1.0 mag above the nominal ZAMS locus, which allows for binarity and some errors in the photometry, reddening and distance modulus. Stars which lie more than 0.4 mag above the ZAMS may be binary systems, although not necessarily close binary systems, and are subsequently labelled as photometric binaries (PhB).

To use the radial velocity information we note that the expected radial velocity dispersion of the cluster members should be of order 1 km s^{-1} (e.g. Stauffer et al. 1997), although the presence of wide binary systems may increase this. The previously determined radial velocity of the cluster is -15 km s^{-1} (Abt et al. 1970; Gieseking 1985) and we clearly have a grouping of measurements around this value. Weighted-mean radial velocities were calculated for each object. Stars with varying radial velocity and photometry consistent with cluster membership are classified as probable spectroscopic binary cluster members, as are those with two components clearly visible in the cross-correlation functions. We note that in all the stars observed in this programme, only three probable single stars have radial velocities between 0 and -10 km s^{-1} and -20 and -30 km s^{-1}. As a criterion for cluster membership we select stars with radial velocities between -10 and -20 km s^{-1}, accepting that one or two spurious objects may be introduced. The stars with appropriate photometry and radial velocities are classified as probable single cluster members. The velocity interval we have chosen is larger than the expected cluster dispersion, and in general larger than the data errors. There are, however, a few rapid rotators with larger error bars that need to be considered. A different approach could be to look for objects within, say, 2σ of an assumed cluster mean velocity after adding 1 km s^{-1} in quadrature to the data errors, but this results in little difference in the final sample selection. Stars which are photometric members but fail the radial velocity test based on only one measurement are classified as possible spectroscopic binaries.

3.2 Spectroscopic and X-ray data

A summary of the spectroscopic data of the X-ray selected sample of NGC 6475 probable single stars, probable binary stars and possible binary stars, is presented in Table 2. The identifier of each star with the J2000.0 right ascension (RA) and declination (Dec.) is listed in columns 1–3. The S/N of each observation, in the velocity-measurement order, is

Table 2. High-resolution observations of an X-ray selected sample of stars in NGC 6475.

Star	R. A. (J2000.0)	Dec. (J2000.0)	S/N	HJD 2449000+	Rad. Vel. km s^{-1}	$v \sin i$ km s^{-1}	Li EW mÅ	Hα EW mÅ	Ca EW mÅ	Comments
				Probable	Single	Cluster	Members			
JJ 1	17 53 37.2	-34 47 49		140.651	-16 ± 5	-	-	-	-	S; K73
JJ 1	-	-		146.596	-15 ± 5	-	-	-	-	S; PhB
JJ 1	-	-	52	198.970	-16.2 ± 0.3	10.3 ± 1.0	124 ± 4	207 ± 5	185 ± 12	A; R61
JJ 2	17 53 22.3	-35 00 31		145.516	-21 ± 6	-	-	-	-	S
JJ 2	-	-	39	199.002	-16.2 ± 0.4	13.0 ± 0.9	105 ± 9	135 ± 7	239 ± 17	A; R42
JJ 3	17 53 55.9	-35 02 28	18	199.904	-15.6 ± 3.4	43 ± 7	58 ± 13	173 ± 20	241 ± 42	A; K87
JJ 3	-	-	24	200.921	-23.8 ± 3.2	36 ± 6	-	-	-	A; R81
JJ 4	17 53 42.4	-35 00 07		140.572	-20 ± 6	-	-	-	-	S
JJ 4	-	-		146.537	-10 ± 6	-	-	-	-	S
JJ 4	-	-	10	199.939	-17.1 ± 0.6	11.5 ± 1.0	30 ± 10	112 ± 26	260 ± 84	A
JJ 4	-	-	13	200.931	-17.1 ± 0.6	-	-	-	-	A; R69
JJ 5	17 53 45.4	-34 46 37		463.847	-10	16	-	-	-	P95
JJ 5	-	-	10	526.214	-17.9 ± 0.8	14.5 ± 1.9	-	290 ± 55	-	M; PhB.?
JJ 5	-	-	11	527.080	-17.8 ± 0.8	18.0 ± 2.0	-	265 ± 48	-	M; R73
JJ 6	17 54 57.7	-34 38 14	34	530.874	-15.4 ± 0.6	19.2 ± 2.4	90 ± 14	121 ± 9	150 ± 19	A; R127b
JJ 7	17 54 55.5	-34 38 28		464.852	-15	< 10	-	-	-	P95
JJ 7	-	-	30	530.897	-15.0 ± 0.3	8.8 ± 1.0	101 ± 9	209 ± 10	215 ± 18	A; R127a
JJ 8	17 54 09.7	-34 53 13	18	530.951	-15.9 ± 0.3	≤ 6	126 ± 10	128 ± 12	258 ± 32	A; R94
JJ 9	17 53 57.1	-34 46 04	20	530.976	-14.9 ± 0.2	≤ 6	127 ± 11	139 ± 12	235 ± 30	A; R82
JJ 10	17 53 54.2	-34 46 08	24	530.995	-14.9 ± 0.2	≤ 6	109 ± 9	124 ± 10	153 ± 19	A; R82
JJ 11	17 53 29.2	-34 48 23	15	531.036	-13.4 ± 0.3	≤ 6	68 ± 12	197 ± 14	203 ± 41	A; R53
JJ 12	17 53 12.0	-34 40 43		465.799	-17	< 10	-	-	-	P95
JJ 12	-	-	19	531.092	-15.7 ± 0.4	9.8 ± 0.9	101 ± 8	100 ± 10	256 ± 20	A; R27
JJ 13	17 52 57.7	-34 56 56		463.927	-12	< 10	-	-	-	P95; R16a
JJ 13	-	-	23	531.218	-14.9 ± 0.3	6.5 ± 1.0	102 ± 7	139 ± 9	271 ± 23	A; PhB
JJ 14	17 52 26.3	-34 35 42	14	531.978	-19.9 ± 0.8	23.8 ± 2.5	123 ± 17	1232 ± 16	691 ± 22	A; R7b
JJ 15	17 52 26.3	-34 35 42	10	532.000	-13.8 ± 1.1	26.9 ± 2.8	203 ± 25	1089 ± 23	773 ± 37	A; R7a
JJ 16	17 53 21.3	-34 54 35		140.575	-19 ± 5	-	-	-	-	S
JJ 16	-	-	22	198.909	-16.5 ± 0.2	≤ 6	116 ± 10	118 ± 11	270 ± 29	A
JJ 16	-	-	6	200.936	-15.5 ± 0.3	-	-	-	-	A
JJ 16	-	-	11	532.090	-15.0 ± 0.2	≤ 6	134 ± 13	106 ± 18	240 ± 39	A; R39a
JJ 17	17 52 50.2	-34 37 19	11	532.183	-17.7 ± 0.6	12.5 ± 1.0	91 ± 11	143 ± 16	240 ± 50	A; PhB
JJ 18	17 52 40.2	-34 37 28	17	532.258	-14.3 ± 0.4	9.8 ± 0.8	124 ± 10	127 ± 11	245 ± 33	A; PhB
JJ 19	17 53 49.0	-34 49 07	18	532.899	-14.9 ± 0.2	≤ 6	104 ± 11	57 ± 17	148 ± 38	A; R76
JJ 20	17 54 34.9	-34 56 55	13	533.006	-14.9 ± 0.3	≤ 6	59 ± 12	134 ± 12	248 ± 12	A
JJ 21†	17 54 35.3	-35 00 57	17	533.057	-10.4 ± 0.3	≤ 6	≤ 9	≤ 11	≤ 20	A; R119b
JJ 22	17 53 08.9	-34 45 52	45	533.147	-15.7 ± 0.4	16.7 ± 2.0	60 ± 8	55 ± 25	97 ± 12	A; R24; K50
JJ 23	17 54 19.1	-34 58 23		140.547	-12 ± 5	-	-	-	-	S
JJ 23	-	-	34	198.953	-15.1 ± 0.2	≤ 6	99 ± 12	150 ± 13	247 ± 40	A
JJ 23	-	-	12	533.266	-15.0 ± 0.4	≤ 6	-	-	-	A; R103
JJ 24	17 53 16.2	-34 42 08	8	1123.267	-14.3 ± 0.5	10.0 ± 1.4	127 ± 18	758 ± 27	364 ± 30	A; R33
JJ 25	17 54 15.6	-34 47 38	8	1125.212	-15.0 ± 0.4	6.3 ± 1.2	108 ± 34	203 ± 16	208 ± 38	A; R102
JJ 26	17 52 46.7	-34 40 59		465.777	-16	< 10	-	-	-	P95
JJ 26	-	-	32	532.020	-15.9 ± 0.2	≤ 6	97 ± 6	104 ± 7	189 ± 13	A; R14
				Probable	Cluster	Binaries				
JJ 27	17 54 20.2	-34 47 44		145.433	-8 ± 5	-	-	-	-	S; one peak
JJ 27	-	-		146.509	-3 ± 5	-	-	-	-	S; one peak
JJ 27	-	-	30	198.986	-4.4 ± 0.3	8.6 ± 1.0	126 ± 8	192 ± 9	300 ± 30	A; R104; SB2
JJ 27	-	-	30	198.986	-28.5 ± 0.3	9.0 ± 1.0	-	-	-	A; SB2
JJ 28	17 53 44.9	-34 50 37		140.634	-22 ± 8	-	-	-	-	S K80
JJ 28	-	-		146.582	-14 ± 8	-	-	-	-	S; SB1
JJ 28	-	-	32	199.871	-28.4 ± 1.6	31 ± 5	59 ± 8	261 ± 10	154 ± 25	A; R72
JJ 29	17 54 09.0	-34 52 19		465.822	-14	< 10	-	-	-	P95
JJ 29	-	-	21	530.931	-11.6 ± 0.3	≤ 6	97 ± 8	117 ± 11	266 ± 26	A; R95
JJ 30	17 52 51.2	-34 52 14		465.875	+24	13	-	-	-	P95; SB1
JJ 30	-	-	29	531.014	+5.3 ± 0.3	12.8 ± 1.1	-	87 ± 10	-	A; R15
JJ 31	17 53 21.5	-34 54 18		140.620	-10 ± 6	-	-	-	-	S
JJ 31	-	-	35	198.932	-58.8 ± 0.3	14.4 ± 1.0	-	215 ± 8	427 ± 19	A

Table 2 – *continued*

Star	R. A. (J2000.0)	Dec. (J2000.0)	S/N	HJD 2449000+	Rad. Vel. km s^{-1}	$v \sin i$ km s^{-1}	Li EW mÅ	Hα EW mÅ	Ca E W mÅ	Comments
JJ 31	-	-		465.842	+20	14	-	-	-	P95; SB1
JJ 31	-	-	25	532.038	+14.1 ± 0.4	13.5 ± 1.2	118 ± 11	153 ± 10	388 ± 26	A; R39b
JJ 32	17 53 28.3	-34 53 58	45	532.275	+43.0 ± 0.4	7.4 ± 2.0	-	96 ± 50	57 ± 50	A; SB2; K61
JJ 32	-	-			-74.5 ± 0.4	7.3 ± 2.0	-	47 ± 50	≤ 50	A; SB2; R50
JJ 33	17 54 36.7	-35 00 51		466.801	-9	< 10	-	-	-	P95; SB ?
JJ 33	-	-			+25	< 10	-	-	-	P95; SB ?
JJ 33	-	-	20	533.035	-14.7 ± 0.2	≤ 6	103 ± 9	242 ± 11	258 ± 36	A; R119a
JJ 34	17 54 26.1	-34 42 14		465.923	-13	< 10	-	-	-	P95; SB1
JJ 34	-	-	26	533.086	-5.6 ± 0.3	7.8 ± 0.9	90 ± 8	299 ± 9	282 ± 26	A; R109
JJ 35	17 53 40.0	-34 40 04		145.589	-6 ± 5	-	-	-	-	S
JJ 35	-	-		466.753	-5	< 10	-	-	-	P95; SB ?
JJ 35	-	-	27	533.116	-11.4 ± 0.3	7.0 ± 1.0	87 ± 7	219 ± 8	375 ± 27	A; R66
				Possible	Cluster	Binaries				
JJ 36	17 55 04.1	-34 57 14	16	199.923	-9.8 ± 0.4	12.0 ± 1.1	49 ± 14	160 ± 16	212 ± 57	A; R132
JJ 37	17 53 08.2	-34 59 09	11	526.129	-10.7 ± 2.7	69 ± 7	-	87 ± 48	-	M; K49
JJ 37	-	-	14	527.006	-6.5 ± 2.5	66 ± 7	-	-	-	M; R22
JJ 38	17 53 31.9	-34 56 22		467.862	-12	70	-	-	-	P95
JJ 38	-	-	11	526.167	-9.3 ± 3.9	81 ± 10	-	193 ± 69	-	M; K67
JJ 38	-	-	15	527.040	-4.1 ± 3.0	86 ± 10	-	209 ± 60	-	M; R56
JJ 39	17 54 46.1	-35 07 02		140.447	+9 ± 7	-	-	-	-	S; R125
JJ 39	-	-	24	531.297	-60	30 ± 10	-	511 ± 70	471 ± 70	A; Hα; SB
JJ 40	17 51 35.1	-34 45 59	10	531.112	-33.2 ± 0.3	≤ 6	17 ± 9	462 ± 16	280 ± 29	A; R1; PhB
JJ 41	17 53 03.2	-35 07 02	26	533.293	-45.9 ± 0.5	10.7 ± 1.3	89 ± 8	114 ± 10	151 ± 20	A
JJ 42	17 55 32.7	-35 26 16	46	532.872	+29.2 ± 0.2	≤ 6	13 ± 4	287 ± 5	-	A; PhB; R134
JJ 43	17 52 59.3	-34 56 57	41	531.204	-32	-	-	-	-	A; R16b; Hα PhB; K45

Notes: Each spectroscopic observation is denoted by A, S or M. This denotes whether the observations were performed using the 3.9-m AAT, 1.9-m SAAO or 1.9-m MSO instrument. The label P95 indicates spectroscopic data from Prosser et al. (1995). The R numbers refer to X-ray sources in the survey by P95. The K numbers indicate a Koelbloed (1995) identification. PhB – photometric binary, SB – spectroscopic binary. JJ 39, JJ 43 – the Hα denotes that the S/N, $v \sin i$ and radial velocity were estimated from their Hα profiles. † Probable non-member, since there is no detectable Li I present and no evidence of chromospheric activity.

listed in column 4 and the heliocentric Julian date (HJD) of each measurement is listed in column 5. The derived radial and rotational velocities are listed in columns 6 and 7, and the Li I 6708-Å and chromospheric Hα and Ca II IRT 8542-Å line EWs are tabulated in columns 8–10. A comments column is supplied to clarify telescope choice, to indicate where the results are quoted by P95, and to identify PhB stars. Cross-identifications with X-ray sources from P95 are also given along with any identifications with stars from the optical survey of Koelbloed (1959). Photometric data are listed for each star in columns 2 and 3 of Table 3. To ensure consistency, all photometric data are taken from P95, Prosser (private communication) or Prosser et al. (1996). These data are plotted on a CMD in Fig. 1, which also shows a ZAMS [solid line, constructed from data presented in Lang 1991, using $d = 250$ pc and $E(B-V) = 0.06$]. The three different subclasses of identification are given different symbols. PSPC count rates for each target are listed in column 9 of Table 3, and are taken from our pointing for the majority of stars. Nine of the targets are either near the edge of our PSPC or pointing or obscured by a supporting rib. For these we have used P95 positions and count rates. We note four pairs (JJ 9 and 10; JJ 14 and 15; JJ 21 and 33; JJ 16 and 31) of cluster members which are associated with a single PSPC source. For each pair, 50 per cent of the PSPC count rate and all of the associated error is allocated to each star. In the case of JJ 21 and JJ 33, we have decided that JJ 21 is a cluster non-member (since it exhibits no detectable Li I or chromospheric activity and its radial velocity only just satisfies our selection criteria) and all the detected X-ray flux is assumed to originate from JJ 33.

3.3 Fluxes and luminosities

Table 3 lists the chromospheric line fluxes, ratios of chromospheric to bolometric emission, X-ray count rates, luminosities and X-ray to bolometric flux ratios for all the spectroscopically investigated stars.

The Hα and the Ca II IRT EWs were converted into line fluxes received at the Earth. Hα fluxes were calculated by transforming $(B-V)_0$ into $(V-R)_0^k$ using equation (1) from S93, and then assuming Kron R_k magnitudes to represent the continuum flux at Hα, given a flux of 2.2×10^{-9} erg cm^{-2} s^{-1} Å^{-1} for $R_k = 0$ (Bessell 1979). Similarly, the Ca II 8542-Å fluxes were calculated by transforming $(B-V)_0$ into $(V-I)_0^J$ using equation (2) from S93, and then assuming Johnson I_J magnitudes to represent the continuum flux at

Table 3. X-ray and chromospheric-line luminosity data for the X-ray selected sample of stars in NGC 6475.

Star	V	(B-V)	$v \sin i$ km s^{-1}	$f_{H\alpha}$ ($\times 10^{-14}$ erg cm^{-2} s^{-1})	f_{IRT}	Log $L_{H\alpha}/L_{bol}$	Log L_{IRT}/L_{bol}	PSPC 10^{-3} ct s^{-1}	Log L_x erg s^{-1}	Log L_x/L_{bol}
				Probable	Single	Members				
JJ 1	11.58	0.68	10.3	1.55 ± 0.04	0.97 ± 0.06	-4.67	-4.88	5.14 ± 0.53	29.84	-3.89
JJ 2	11.38	0.63	13.0	1.17 ± 0.06	1.41 ± 0.10	-4.87	-4.79	3.79 ± 0.43	29.71	-4.10
JJ 3	11.38	0.54	39	1.43 ± 0.16	1.28 ± 0.22	-4.78	-4.82	2.83 ± 0.47	29.58	-4.23
JJ 4	12.13	0.66	11.5	0.50 ± 0.12	0.80 ± 0.26	-4.94	-4.74	1.81 ± 0.35	29.39	-4.13
JJ 5	10.95	0.57	16	3.46 ± 0.64	-	-4.57	-	5.92 ± 0.58	29.90	-4.08
JJ 6^{I}	11.67	0.63	19.2	0.74 ± 0.05	0.62 ± 0.06	-4.95	-5.03	5.52 ± 0.96	29.87	-3.82
JJ 7^{I}	11.88	0.67	8.8	1.08 ± 0.05	0.76 ± 0.06	-4.71	-4.86	5.02 ± 0.86	29.83	-3.78
JJ 8	13.30	0.87	$\leq$ 6	0.22 ± 0.02	0.35 ± 0.04	-4.88	-4.68	1.23 ± 0.32	29.22	-3.87
JJ 9	12.87	0.73	$\leq$ 6	0.33 ± 0.03	0.40 ± 0.05	-4.84	-4.76	1.59 ± 0.46	29.33	-3.91
JJ 10‡	12.53	0.74	$\leq$ 6	0.40 ± 0.03	0.36 ± 0.04	-4.90	-4.95	1.59 ± 0.46	29.33	-4.04
JJ 11	13.40	0.90	$\leq$ 6	0.32 ± 0.02	0.13 ± 0.03	-4.68	-5.09	2.13 ± 0.36	29.46	-3.60
JJ 12	12.12	0.68	9.8	0.45 ± 0.05	0.81 ± 0.06	-4.94	-4.68	1.41 ± 0.38	29.28	-4.19
JJ 13	11.69	0.72	6.5	0.96 ± 0.06	1.34 ± 0.11	-4.85	-4.70	2.57 ± 0.41	29.54	-4.17
JJ 14	13.78	1.08	23.8	1.64 ± 0.02	0.76 ± 0.02	-3.88	-4.22	6.22 ± 0.98	29.92	-3.05
JJ 15	14.15	1.06	26.9	1.02 ± 0.02	0.59 ± 0.03	-3.93	-4.17	6.22 ± 0.98	29.92	-2.89
JJ 16	12.36	0.71	$\leq$ 6	0.42 ± 0.07	0.67 ± 0.09	-4.94	-4.73	1.95 ± 0.49	29.42	-4.01
JJ 17‡	12.30	0.75	12.5	0.58 ± 0.06	0.70 ± 0.15	-4.83	-4.75	1.36 ± 0.41	29.26	-4.21
JJ 18	11.99	0.77	9.8	0.69 ± 0.06	0.97 ± 0.13	-4.88	-4.73	1.79 ± 0.47	29.38	-4.22
JJ 19	13.55	0.95	$\leq$ 6	0.08 ± 0.03	0.17 ± 0.04	-5.24	-4.90	1.97 ± 0.36	29.42	-3.59
JJ 20‡	14.05	1.04	$\leq$ 6	0.13 ± 0.01	0.20 ± 0.01	-4.86	-4.66	15.56 ± 4.68	30.32	-2.52
JJ 21	13.46	0.91	$\leq$ 6	$\leq$ 0.02	$\leq$ 0.02	-5.86	-5.79	-	-	-
JJ 22	11.11	0.50	16.7	0.57 ± 0.26	0.63 ± 0.08	-5.28	-5.24	1.67 ± 0.34	29.35	-4.56
JJ 23†	12.37	0.71	$\leq$ 6	0.55 ± 0.05	0.65 ± 0.10	-4.81	-4.74	3.80 ± 0.60	29.71	-3.72
JJ 24	13.42	0.89	10.0	1.21 ± 0.04	0.45 ± 0.04	-4.09	-4.53	4.09 ± 0.48	29.74	-3.31
JJ 25†	13.32	0.89	6.3	0.35 ± 0.03	0.28 ± 0.05	-4.67	-4.77	2.10 ± 0.30	29.45	-3.64
JJ 26	12.06	0.66	$\leq$ 6	0.49 ± 0.03	0.62 ± 0.04	-5.16	-5.06	3.36 ± 0.49	29.65	-4.07
				Probable	Cluster	Binaries				
JJ 27	12.37	0.82	8.8	0.76 ± 0.04	0.89 ± 0.09	-4.70	-4.63	5.04 ± 0.63	29.83	-3.63
JJ 28	10.79	0.55	31	3.72 ± 0.14	1.43 ± 0.23	-4.60	-5.01	11.71 ± 0.73	30.20	-3.85
JJ 29	12.19	0.68	$\leq$ 6	0.50 ± 0.05	0.79 ± 0.08	-4.92	-4.72	1.57 ± 0.31	29.33	-4.17
JJ 30†	12.28	0.71	12.8	0.35 ± 0.04	-	-5.05	-	1.90 ± 0.60	29.41	-4.06
JJ 31	12.19	0.69	14.0	0.79 ± 0.04	1.23 ± 0.07	-4.72	-4.53	1.95 ± 0.46	29.42	-4.07
JJ 32	9.65	0.44	7.4	3.68 ± 0.20	1.33 ± 0.21	-5.06	-5.50	1.69 ± 0.33	29.36	-5.15
			7.3	1.80 ± 0.11	$\leq$ 0.26	-5.37	-6.22	"	"	"
JJ 33†	12.92	0.81	$\leq$ 6	0.57 ± 0.03	0.46 ± 0.06	-4.60	-4.70	1.80 ± 0.70	29.38	-3.85
JJ 34†	12.63	0.80	7.8	0.92 ± 0.03	0.64 ± 0.06	-4.51	-4.67	2.00 ± 0.30	29.43	-3.92
JJ 35†	12.78	0.78	7.0	0.58 ± 0.02	0.73 ± 0.05	-4.65	-4.55	1.30 ± 0.30	29.24	-4.04
				Possible	Cluster	Binaries				
JJ 36†	11.81	0.68	12.0	0.97 ± 0.01	0.90 ± 0.24	-4.78	-4.82	4.90 ± 0.40	29.82	-3.82
JJ 37	10.63	0.45	68	1.36 ± 0.75	-	-5.10	-	1.40 ± 0.33	29.27	-4.83
JJ 38	10.66	0.43	83	3.01 ± 0.98	-	-4.75	-	1.83 ± 0.34	29.39	-4.71
JJ 39†	11.28	0.68	30	5.03 ± 0.50	3.24 ± 0.26	-4.28	-4.47	7.00 ± 1.00	29.97	-3.88
JJ 40^{II}	13.30	1.13	$\leq$ 6	1.02 ± 0.04	0.52 ± 0.05	-4.30	-4.59	11.26 ± 0.97	30.18	-3.00
JJ 41	11.57	0.58	10.7	0.81 ± 0.07	0.71 ± 0.09	-4.95	-5.01	1.30 ± 0.45	29.24	-4.48
‡JJ 42†	12.41	0.84	$\leq$ 6	1.12 ± 0.02	-	-4.52	-	39.00 ± 2.00	30.72	-2.72
JJ 43	9.36	0.35	-	-	-	-	-	1.37 ± 0.33	29.26	-5.37

Notes: †PSPC count rates are from P95. ‡Indicates the V and $(B-V)$ photometry are from Prosser (private communication). All other listed photometry data are taken from P95, except where indicated. I – Photometry taken from Prosser et al. (1996). II – There is no $(B-V)$ value yet available for this star. The quoted value in the table has been calculated from its $(V-I)_c$ value (P95), using a linear fit to the $(B-V)$, $(V-I)_c$ data presented in Menzies & Marang (1996). Bolometric luminosities calculated assuming $E(B-V)=0.06$; bolometric corrections are taken from Zombeck (1990).

8500 Å, given a flux of 8.32×10^{-10} erg cm^{-2} s^{-1} Å^{-1} for $I_J=0$ (Johnson 1966),

$$(V-R)_0^k=0.283(B-V)_0^2+0.361(B-V)_0-0.106, \quad (1)$$

$$(V-I)_0^J=1.272(B-V)_0+0.105. \quad (2)$$

Some systematic error is probable because the R_k and I_J filters have approximate effective wavelengths of 6500 and 9000 Å (Johnson 1966; Bessell 1979). This will not greatly affect the derived values, and since all cluster members and comparison stars in other clusters (see Section 4.1, below)

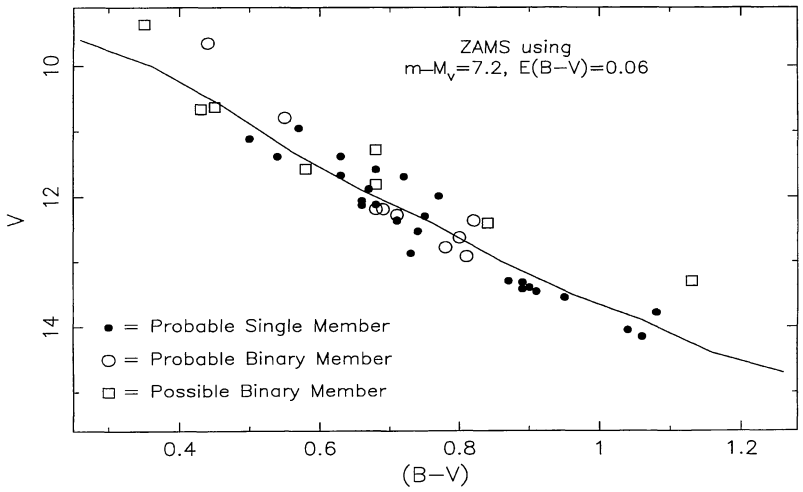

Figure 1. The zero-age main sequence of NGC 6475, using a distance modulus of 7.2 and a reddening of $E(B-V)=0.06$, is plotted (constructed from data in Lang 1991). All probable single (filled circles), probable binary (open circles) and possible binary (open squares) members of the cluster observed spectroscopically are plotted (see Tables 2 and 3).

were treated equivalently, comparisons between clusters are valid.

PSPC count rates were converted to fluxes at the Earth using the conversion factors calculated in Section 2.1. X-ray luminosity, L_X, is calculated assuming a common distance of 250 pc. Clearly, X-ray luminosities for those sources which are not bona fide members of the cluster will be incorrect. Magnetic activity is often expressed as a ratio of the flux in a particular waveband or spectral line to the bolometric flux. These ratios have been calculated for the chromospheric ($L_{H\alpha}/L_{bol}$, L_{IRT}/L_{bol}) and X-ray (L_X/L_{bol}) fluxes from each star, using bolometric corrections from Zombeck (1990).

3.4 The metallicity of NGC 6475

A comparison of confirmed spectra of cluster members to synthesized spectra generated by a model atmosphere code has enabled us to estimate the metallicity [Fe/H] of several individual cluster members. We have synthesized spectra in the region between 5681 and 5721 Å in the AAT spectra. We used Kurucz model atmospheres (Kurucz 1991), the Kurucz & Bell (1995) line list and the UCLSYN synthesis software (Smith 1992) to generate spectra at a range of metallicities. Stellar temperatures (T_{eff}) have been calculated using $E(B-V)=0.06$ and the $T_{eff}-(B-V)$ relation from S93; gravities are taken from the T_{eff}-log g data given in Gray (1992). We have used a microturbulence (ξ) of 2 km s^{-1} for all the targets, consistent with values of $\xi=1$–2 km s^{-1} reported elsewhere for solar-type stars (Boesgaard & Friel 1990; Soderblom et al. 1993b). The observational spectra have been chosen from the probable single cluster members, as long as they have reasonably good S/N and are not photometric binaries. The mean metallicity of the cluster is [Fe/H] $= +0.080 \pm 0.046$. The stars used to evaluate the metallicity, their adopted effective temperatures and gravities, and their derived [Fe/H] values are presented in Table 4. The quoted error includes an error on the mean and an assumed error of 0.03 in the mean reddening.

Table 4. Effective temperature, gravity and derived [Fe/H] of a sample of NGC 6475 cluster members. $\xi=2$ km s^{-1} has been used for each star.

Star	T_{eff} K	log g cm s^{-2}	[Fe/H]
JJ 2	6007	4.41	+0.13 ± 0.05
JJ 4	5888	4.44	+0.16 ± 0.05
JJ 6	6089	4.40	+0.09 ± 0.05
JJ 7	5967	4.42	−0.22 ± 0.05
JJ 8	5142	4.55	+0.09 ± 0.05
JJ 9	5622	4.48	+0.12 ± 0.05
JJ 10	5585	4.48	+0.03 ± 0.05
JJ 12	5810	4.45	+0.13 ± 0.05
JJ 19	4900	4.59	+0.13 ± 0.05
JJ 22	6563	4.31	+0.12 ± 0.05
JJ 26	5888	4.44	+0.10 ± 0.05

The anomalous metallicity of JJ 7 (situated in the north-west corner of the cluster) indicates that it is either a cluster non-member, a chemically peculiar member or a more heavily reddened cluster member. Photometric and radial velocity measurements of JJ 7 (see Tables 2 and 3) indicate it is a bona fide cluster member; furthermore, it also shows cluster-like Li I, Hα and 8542-Å IRT properties (see Table 2). The star may be chemically peculiar although our AAT spectra do not appear (by eye) to be significantly different from the spectra of other cluster members. However, during the spectral syntheses, we tried incrementing the effective temperature and corresponding log g of the models to investigate whether a significant increase in the stellar effective temperature would yield a cluster-like metallicity. We find an atmospheric model with $T_{eff}=6330$ K $[(B-V)_0=0.46]$ and log $g=4.35$ results in a good fit to the observed spectrum, with a cluster metallicity of [Fe/H] ~ 0.1. The observed $(B-V)$ of JJ 7 is 0.67; therefore, if the star is indeed a bona fide cluster member, a reddening of $E(B-V)=0.21$ is inferred. This finding suggests differential reddening across the cluster, consistent with the results

of the four-colour Stromgren photometry survey among brighter ($V \lesssim 11$) members of the cluster by Snowden (1976). If differential reddening is the true cause of the anomalous [Fe/H] value, it must be fairly localized because JJ 7 is only 30 arcsec from JJ 6. If we do not include the [Fe/H] value of JJ 7, we find, and hereafter adopt, a metallicity of [Fe/H] $= +0.110 \pm 0.034$.

4 COMPARISON WITH OTHER CLUSTERS

4.1 Comparison data

The evolution of rotation, magnetic activity, and lithium abundance is best examined by comparing our new data on members of NGC 6475 with stars of similar spectral types in other open clusters. The Pleiades and Hyades are the obvious comparisons, since the age of NGC 6475 is in between the two. The Ursa Major moving Group (UMa Group, age 300 Myr – Soderblom & Mayor 1993) is also considered, to investigate whether stars at similar ages can exhibit significant physical differences. The convection zone depth and base temperature are metallicity dependent and so cluster-to-cluster metallicity variations might confuse evolutionary trends governed by convective processes such as the magnetic dynamo or mixing (e.g. Chaboyer et al. 1995; Jeffries et al. 1997). The metallicities and adopted ages of the comparison clusters (from Friel & Boesgaard 1992) and NGC 6475 are detailed in Table 5. The metallicity of the Hyades and NGC 6475 are approximately equal, and similar colour stars in each cluster are expected to have similar physical characteristics.

4.1.1 *Spectroscopic/photometric data*

Chromospheric activity, photometric data and $v \sin i$ measurements for the Pleiades are taken from S93 (and references therein). Li I 6708-Å EWs are taken from Soderblom et al. (1993b). None of the chosen Pleiads show firm evidence of spectroscopic binarity. We have also avoided using Pleiads situated in the region of anomalous reddening identified by Breger (1986). Chromospheric activity data for the Hyades have not been included because of the lack of a uniform data set analysed by the spectral subtraction technique. There also appears to be no Ca II IRT data available for Hyades stars in the literature. Li I 6708-Å EWs and photometric data for the Hyades are taken from Soderblom et al. (1990) and Thorburn et al. (1993). Measurements of $v \sin i$ for the Hyades are generally upper limits, apart from a few M dwarfs. We have chosen to use the Hyades mean relationship (HMR) between true equatorial velocity (V_{eq}, calculated from rotation periods) and $B-V$, presented by S93. There is a small scatter of <15 per cent about the HMR for late-F, G and K dwarfs (Radick et al. 1987). Again, our choice of comparison stars in the Hyades is restricted to those with no evidence for spectroscopic binarity. The chromospheric, photometric and $v \sin i$ data for the UMa group stars are taken from Soderblom & Mayor (1993) and the Li I 6708-Å EWs are taken from Soderblom et al. (1993c). Spectroscopic binary members of the group are not included.

Table 5. Adopted ages and metallicities for NGC 6475, and the comparison open clusters (ages are from sources cited in the text). [Fe/H] data for the comparison clusters are taken from Friel & Boesgaard (1992).

Cluster	Age *Myr*	[Fe/H]
Pleiades	70	-0.034 ± 0.024
NGC 6475	220	$+0.110 \pm 0.034$
UMa Group	300	-0.086 ± 0.021
Hyades	600	$+0.127 \pm 0.022$

4.1.2 *X-ray data*

The Pleiades X-ray data are taken from the deep PSPC observation of the cluster by Stauffer et al. (1994). X-ray fluxes and luminosities were derived in the 0.15–2.0-keV energy range, using a 1-keV thermal spectrum with interstellar absorption, $N_H = 10^{20.5}$ cm^{-2}, and a CF of 1 count s$^{-1} \equiv 1.2 \times 10^{-11}$ erg cm^{-2} s^{-1}. The Hyades X-ray data are taken from two separate sources. Two-thirds of the sample is from the *ROSAT* All Sky Survey (RASS) PSPC data (Stern et al. 1992). Fluxes and luminosities in the 0.1–2.4-keV energy range were calculated assuming negligible interstellar absorption and a CF of 1 count s$^{-1} \equiv 6.0 \times 10^{-12}$ erg cm^{-2} s^{-1}. The remaining third of the sample is from the deep PSPC observation of the cluster by Stern et al. (1994) using the RASS energy range and CF. X-ray data for stars in the UMa Group are taken from source detections using the Imaging Proportional Counter (IPC) on board the *Einstein* Observatory. IPC X-ray luminosities were derived in the 0.16–4.0-keV energy band, using a standard *Einstein* CF of 1 count s$^{-1} \equiv 2.0 \times 10^{-11}$ erg cm^{-2} s^{-1}, appropriate for source temperatures $\geq 3 \times 10^6$ K and negligible interstellar absorption (Schmitt et al. 1990).

The comparability of X-ray data between different clusters may be compromised by various systematic errors. Uncertainties in cluster distances are bypassed by using L_X/L_{bol} as the primary activity indicator. The various literature sources use differing bolometric correction calibrations, but this is of negligible importance in the colour range of stars considered here. The differing energy ranges used in the Pleiades and UMa Group observations also result in reasonably small discrepancies. Of more importance are the assumptions made concerning the temperatures of coronal plasmas and absorbing column densities. We can show, for example, that the luminosities of NGC 6475 can be altered by about ± 30 per cent for changes in the absorbing column density within the error bars of our spectral fitting. Similar sized discrepancies may also result from uncertainties in the assumed coronal temperatures.

4.2 Rotation

When discussing the rotation data for NGC 6475 compared with other clusters, two important observational biases should be kept in mind. First, our sample is X-ray-selected at a threshold that we will show (in Section 4.3) is below the X-ray saturation limit found by Stauffer et al. (1994) for G and K stars, but is above that of the least-active stars in the Pleiades. Secondly, as NGC 6475 is older than the Pleiades,

we expect there to be many X-ray undetected late-type members of NGC 6475, resulting in a strong bias against the spectroscopic observation of slowly rotating stars in the cluster. This bias is not present in the other samples as they have been selected on photometric, radial velocity or proper motion grounds. However, our spectroscopic sample does include eight of the nine most active G star candidates (as judged by L_X/L_{bol}) in the X-ray/photometric survey of P95, as well as three of the four most active K star candidates. It is therefore likely that our results include the most rapidly rotating G and K stars in the cluster, although saturation of the K star X-ray emission may confuse matters (see Section 4.3).

The $v \sin i$ data of late-type stars (late-F→K4) in NGC 6475 and the comparison clusters are plotted against intrinsic colours in Fig. 2. Approximate spectral types, annotated on the abscissa, are estimated from the data presented in Gray (1992). The HMR is also plotted. All rotation velocities, apart from the HMR, are $v \sin i$ measurements and therefore lower limits to the true equatorial rotation velocities.

Binarity can also be a confusing factor when studying rotation periods. Tidal locking in short-period binary systems enforces rapid rotation. We treat those stars suspected of being probable spectroscopic binary members of NGC 6475 separately from those which are nominally single. We do not consider the possible binary members as sufficiently secure identifications. Similarly, we have made efforts to only include those stars without evidence of spectroscopic binarity in the comparison samples from other clusters.

4.2.1 *Late-F stars – $(B-V)_0$=0.48–0.58*

Observations of late-F stars in the Pleiades and Hyades provide some evidence for spin-down during their first 550 Myr on the MS. The range in Pleiad $v \sin i$ values is ∼15–70 km s^{-1} whereas the Hyades have maximum equatorial velocities (calculated from rotational periods) of ∼12 km s^{-1}. Although there are only five NGC 6475 data points in this colour interval, some rotational evolution is apparent during the residence of the stars on the MS between the Pleiades, NGC 6475 and the Hyades. The range of $v \sin i$ in NGC 6475 late-F dwarfs is ≤10–40 km s^{-1}, indicating that some of these stars are rotating more rapidly than their counterparts in the Hyades.

4.2.2 *G stars – $(B-V)_0$=0.58–0.82*

There are two striking phenomena immediately apparent in the observed G star $v \sin i$ distributions in the α Per, Pleiades and Hyades clusters (see fig. 1 of Stauffer 1991). First, spectroscopic rotational velocities obtained for G stars in the α Per and Pleaides clusters have provided evidence for some significant spin-down, and $v \sin i$ convergence, in these stars in ∼20 Myr. Secondly, the rotational velocity distribution of G stars by the age of the Hyades is essentially a single-valued function of mass, with little intrinsic scatter. Thus, distinct physical processes must occur to enable rapid G star AML in ∼20 Myr, and to cause near-complete convergence of surface rotation rates in these stars after ∼500 Myr on the MS.

We proceed using the assumption that the Pleiades $v \sin i$ distribution is formed as a direct evolution of the rotation distribution in α Per, and evolves along the MS to form the $v \sin i$ distribution of stars at 220 Myr. The range of true equatorial velocities (derived from photometric period data) in α Per G stars is ∼7–200 km s^{-1}, and ∼5–50 km s^{-1} in the Pleiades, although more noteworthy is the fact that only ∼20 per cent of G-star Pleiads are UFRs compared to ∼50 per cent in α Per. If this apparent rapid spin-down phase continues beyond the Pleiades age, then naively we might expect all G stars in NGC 6475 to have completely spun-down, with $v \sin i \leq 6$ km s^{-1}. We have observed NGC 6475 G stars with $v \sin i$ between ≤6 and ∼13 km s^{-1} (see Fig. 2), and MS spin-down is *not* complete by 220 Myr. The most rapid G stars in the cluster are still rotating twice as fast as the slowest counterparts in the α Per, Pleiades and Hyades clusters. We note that there are two early-G stars in NGC 6475 which lie below the HMR, but this may simply be the result of small inclination angles. We cannot comment

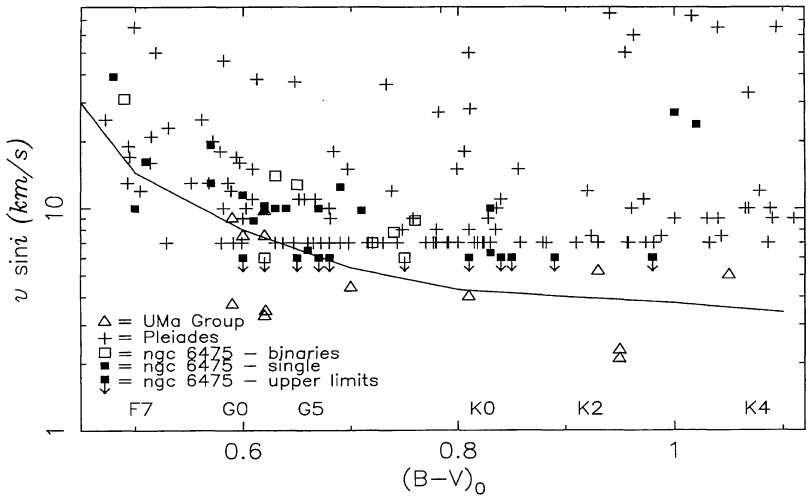

Figure 2. Observed $v \sin i$ versus intrinsic colours are plotted for late-F to K4 stars in the Pleiades, Ursa Major moving Group and NGC 6475. Approximate spectral types are annotated above the abscissa. The majority of the Pleiades measurements at 7 km s^{-1} are upper limits, and the solid line represents the mean Hyades $(B-V)$–$v \sin i$ relation (taken from S93).

any further on the rotation distribution of the G stars in NGC 6475, because of the inherent bias in the sample selection.

Rotational velocity data for UMa Group G stars are claimed to fit into the existing rotation–age relationship established from open cluster observations (Soderblom & Mayor 1993). If these observations had been done using the AAT, the results would have indicated that only three out of seven UMa Group G stars had $v \sin i \leq 6$ km s^{-1}, compared with 10 out of 14 in NGC 6475. Furthermore, the peak UMa group $v \sin i$ is < 10 km s^{-1} and X-ray activity levels lie within the X-ray distribution of the Hyades (see Section 4.3). We would conclude that it is likely that the UMa Group G stars are actually rotating more slowly than the fastest Hyads. It may also be possible that a large age spread exists within the group, or that the sample is not truly representative of a group of stars with an age of 300 Myr because of significant field star contamination (Schmitt et al. 1990).

Five out of seven G star probable spectroscopic binaries in NGC 6475 are rotating with $v \sin i > 6$ km s^{-1}, compared with 10 out of 14 single stars. So despite the probability of tidal synchronization of the components, we have no evidence for enhanced rotation in the binary systems.

4.2.3 K stars – $(B-V)_0 = 0.82$–1.10

The observed spin-down amongst α Per and Pleiades G stars is less obvious in lower mass stars. For K stars, the range of true V_{eq} in both the α Per and Pleiades is $\sim$7–180 km s^{-1}, and the relative percentages of UFRs in the two clusters are similar ($\sim$50 per cent). Therefore, the $v \sin i$ distributions of G and K stars in young clusters indicate that K star spin-down time-scales are longer than those of G stars. Longer spin-down time-scales with decreasing mass are also implied from the Hyades velocity distribution, because the G and K Hyad velocity distribution is a single-valued function of mass, with little intrinsic scatter, yet some UFRs are found among the M-dwarf Hyades (as is one late-K star). Assuming we have observed the most rapidly rotating stars in the cluster, the $v \sin i$ distribution of early-K stars in NGC 6475 ($\leq$6–10 km s^{-1}) is indicative of significant spin-down and convergence after $\sim$150 Myr residence on the MS. The magnitude of the apparent spin-down may be significantly smaller if these stars are rotating more rapidly because of low inclination angles. This hypothesis is not supported by the X-ray data (cf. Fig. 3), which indicate that all observed early-K stars in the cluster are rotating below the threshold rotation for X-ray saturation, of $\sim$15 km s^{-1}, since all of these stars have $L_X/L_{bol} < 10^{-3}$. The degree of spin-down is less clear in the mid-K stars because we have discovered two UFRs in the cluster, both with saturated levels of X-ray emission ($L_X/L_{bol} \sim 10^{-3}$ – see Fig. 3).

The V_{eq} distribution of K stars in the α Per, Pleiades and Hyades clusters implies that the spin-down time-scale for K stars is > 20 and < 600 Myr. Assuming that the measured $v \sin i$ of the UFR target, JJ 15, is $\leq V_{eq}$, mid-K stars appear to spin-down from $V_{eq} \sim 180$ km s^{-1} to $V_{eq} \geq 27$ km s^{-1} as they evolve along the MS from the Pleiades to NGC 6475. If AML mechanisms operate with physical characteristics which remain consistent over several spin-down time-scales, then these data argue in favour of a minimum mid-K star spin-down (e-folding) time-scale of $\sim$75 Myr, and a period of > 150 Myr to achieve the full convergence apparent in the Hyades K stars.

4.3 Magnetic activity

Among cool stars ($T_{eff} \leq 6500$ K), stellar magnetic field production increases with increasing stellar rotation rate, via the dynamo process. Greater magnetic heating of plasma in the outer atmosphere of the star results in higher levels of radiative losses from the plasma. Observations of late-type dwarfs, both in the field and in open clusters, are in agreement with this picture of magnetic activity, and enhanced levels of coronal (Hempelmann et al. 1995) and to a lesser extent, chromospheric (Robinson et al. 1994) emission are evident with increasing rotation rate. Chromospheric and coronal flux data indicate that, above a characteristic velocity of $\sim$15 km s^{-1}, emission levels do not increase with increasing rotation rates, and appear to *saturate*, possibly indicating a saturated state in the stellar dynamo. Recent

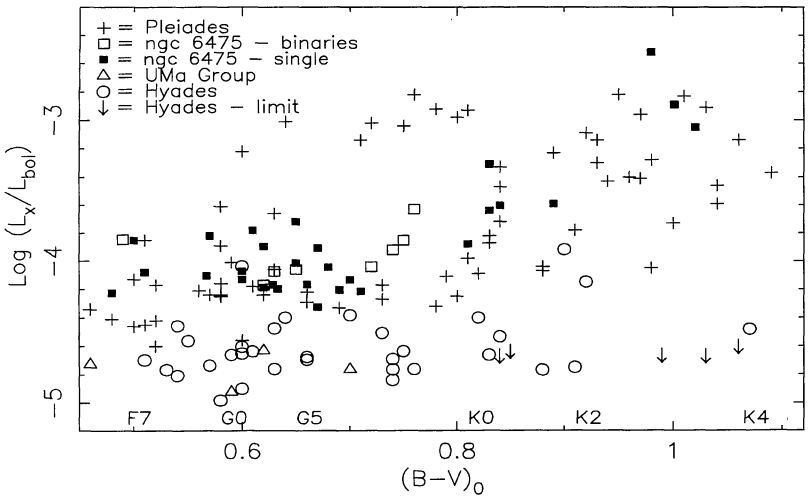

Figure 3. X-ray luminosity as a fraction of the total luminosity is plotted against intrinsic colour for late-F to K4 stars in the Pleiades, Ursa Major moving Group, Hyades and NGC 6475.

observations of late-type dwarfs in the Pleiades reveal levels of saturated chromospheric emission, using the IRT line flux at 8542 Å and the Hα line flux, for $v \sin i > 15$ km s^{-1} (S93). At X-ray wavelengths, a similar flux saturation is observed and L_X/L_{bol} appears to saturate at $\simeq 10^{-3}$ in young open cluster stars with $v \sin i \sim 10$–20 km s^{-1} (Stauffer et al. 1994).

X-ray, Hα and Ca II IRT activity as a function of intrinsic colour are presented in Figs 3, 4 and 5, for both NGC 6475 and the comparison clusters. The behaviour of late-type star coronal activity in NGC 6475 appears correlated with rotation in the sense that all G and early-K stars in the cluster have $L_X/L_{bol} < 10^{-3}$, indicative of rotation rates $\lesssim 15$ km s^{-1}, in agreement with their measured $v \sin i$ and arguing against the possibility of very low inclination angles in the most rapid rotators. Furthermore, only three targets (all of which are mid-K stars) have saturated levels of X-ray emission, and two of these (JJ 14 and JJ 15 – see below for discussion of JJ 20) are rotating with $v \sin i > 20$ km s^{-1}. All observed single and binary stars in NGC 6475 exhibit coronal activity levels in excess of their Hyad counterparts (except one), but overlap to some extent with the Pleiades distribution. This agrees with the measured rotation rate distribution in the two clusters. Unfortunately we cannot argue that this implies there are no NGC 6475 stars rotating more slowly than their Hyades counterparts, because the X-ray sample is flux limited. It is still possible that more slowly rotating and less magnetically active NGC 6475 members exist.

The majority of G and early-K stars in NGC 6475 exhibit chromospheric emission levels below their Pleiades counterparts, indicative of lower mean rotation rates. There is some indication that the chromospheric activity levels of the probable binary systems are higher than those of single stars. Furthermore, our results show that $L_{H\alpha}/L_{bol}$ and L_{8542}/L_{bol} reach maximum values of $\sim 10^{-4}$ and $10^{-4.2}$ respectively, comparable with saturated levels of chromospheric activity in late-type Pleiads (S93). A general coronal–chromospheric activity correlation exists amongst single, late-type cluster members, and is plotted in Fig. 6. A single-order

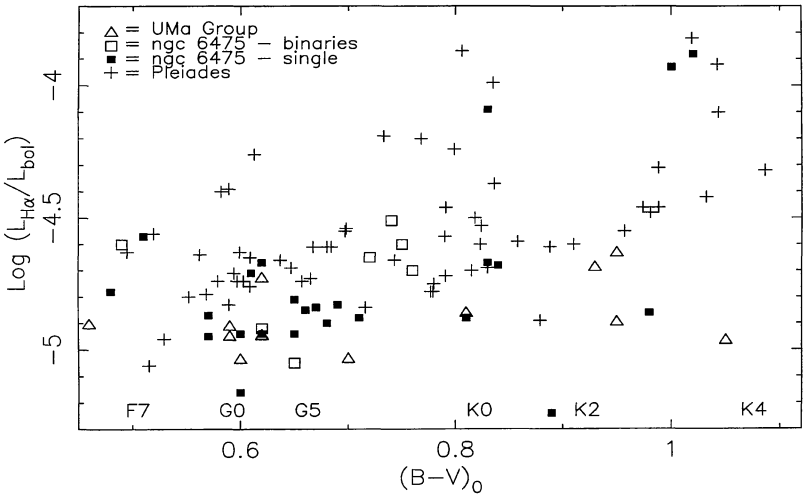

Figure 4. Chromospheric Hα luminosity as a fraction of the total luminosity is plotted against intrinsic colour for late-F to K4 stars in the Pleiades, Ursa Major moving Group and NGC 6475.

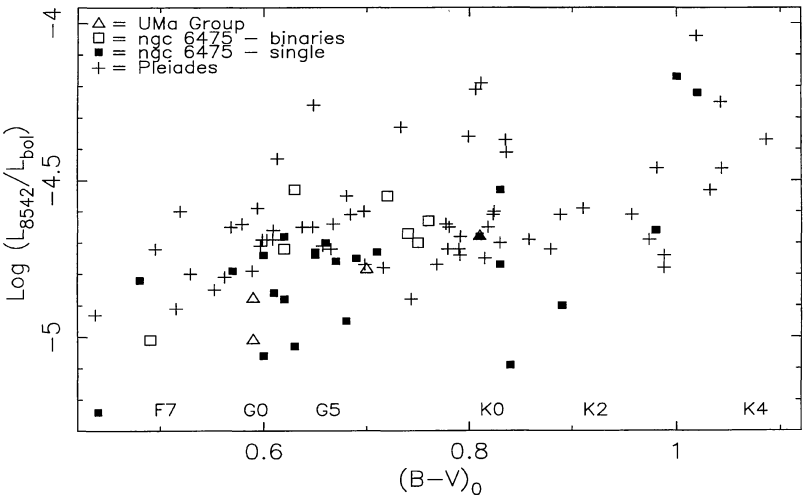

Figure 5. Chromospheric Ca II 8542-Å IRT luminosity as a fraction of the total luminosity is plotted against intrinsic colour for late-F to K4 stars in the Pleiades, Ursa Major moving Group and NGC 6475.

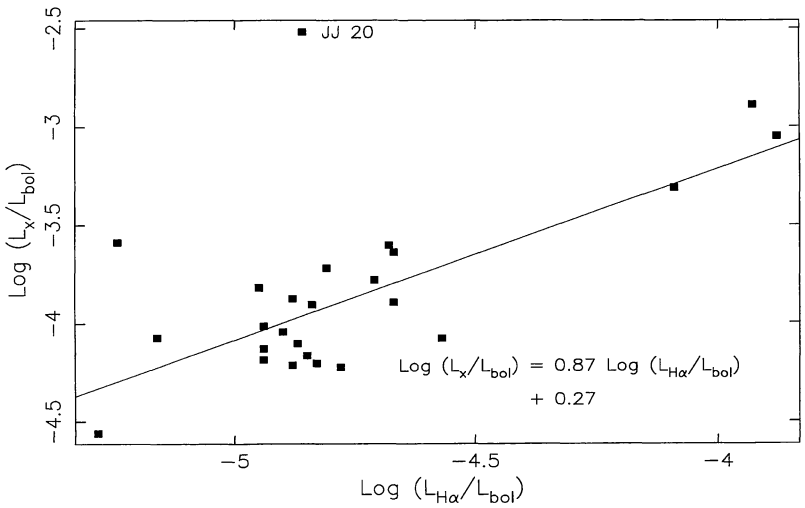

Figure 6. The correlation of coronal versus chromospheric activity of single late-type stars in NGC 6475 is presented. The solid line indicates a first-order polynomial fit to the data (except JJ 20 point at $L_{X/L_{bol}} \sim -2.5$); the fitting coefficients are annotated in the bottom right corner.

polynomial has been fitted to the data (solid line in the plot; fit excludes point with $L_X/L_{bol} \sim -2.50$), yielding $L_X/L_{bol} = 7.4\, L_{H\alpha}/L_{bol} + 1.9$. This correlation is not excellent on a star-to-star basis, but generally, higher levels of coronal activity are observed for more chromospherically active stars.

We note that the mid-K target, JJ 20 (see Fig. 6), has an extremely high L_X/L_{bol}, and a measured rotation of ≤ 6 km s^{-1}. If the star is a low-inclination object, its true velocity may be far higher, consistent with the saturated level of X-ray emission. However, the level of chromospheric activity in this object is surprisingly modest if the star is a rapid rotator. The coronal and chromospheric observations are not co-temporal, and it is possible we have observed the star in a high activity or flare state. A time series of the PSPC observations of this object was constructed but no evidence for a flare was apparent. However, long-duration X-ray flares, detected on the RS CVn binary CF Tuc, have been shown to have lifetimes of ~ 9 d (Kürster & Schmitt 1996), and it is possible the object was in a flare state for the duration of our PSPC observation. During our PSPC analyses, only one source was detected in the soft band. The position of the source was co-incident with JJ 20. The radial velocity and photometry of JJ 20 are consistent with a single cluster member on the MS. An extremely X-ray active cluster member may exhibit sufficiently high levels of X-ray emission in the soft band that would not be completely absorbed by interstellar hydrogen. For such a target, the ratio of hard band to soft band counts would be $\gg 1$. However, the ratio of counts in the hard band to the soft band, for this source, is ~ 1, and it is probable that not all of the detected X-ray flux is associated with a cluster member. We conclude that although JJ 20 is a probable cluster member, it is unlikely to be the *only* object responsible for the detected X-ray emission.

4.4 Lithium in NGC 6475

Lithium abundances of late-F to K4 stars in the Pleiades, Hyades, UMa Group and NGC 6475 are plotted against effective temperatures in Fig. 7. Li I 6708-Å EWs have been converted to abundances using the curves of growth in Soderblom et al. (1993b). The undepleted cosmic abundance, assumed to be N(Li) = 3.2 (following Soderblom et al. 1993b), is also plotted (dashed line). Very little Li depletion has occurred by the age of the Pleiades (between ~ 0.2–0.4 dex below the cosmic abundance), although abundances of some later-G stars do appear to lie up to 1 dex below the undepleted cosmic abundance. These stars have already settled on the MS and we cannot say whether PMS and/or MS depletion has occurred. However, the early-G stars in the Hyades exhibit more Li depletion than do their counterparts in the Pleiades, indicating that these G stars may have experienced some MS depletion, although the increased metallicity and deeper convection zones of the Hyades could also have enhanced PMS depletion with respect to the Pleiades (Swenson et al. 1990; Chaboyer et al. 1995). This effect is more obvious in the Hyades mid/late-G stars which exhibit abundances more than an order of magnitude below Pleiades stars at $T_{eff} \sim 5300$ K.

The Li depletion in young open cluster early/mid-K stars appears very different from the G star lithium depletion pattern. By the age of the Pleiades, K stars have just arrived on the MS [M = 0.7 $M_\odot$, $T_{eff} \sim 4500$ K (K4), time to reach the MS, τ_{ZAMS}, is $\simeq 69$ Myr – Pinsonneault, Kawaler & DeMarque 1990], and their Li abundances indicate that, in some cases, substantial PMS depletion has taken place. Early-K stars in the Hyades cluster have experienced extensive MS and/or PMS Li depletion, with abundances 2–3 orders of magnitude below their counterparts in the Pleiades; and with approximately half the K Hyad detections reported as EW upper limits (there is no detectable Li for $T_{eff} \lesssim 4900$ K), the depletion may be even greater.

Our observations go some way to resolving the relative importance of MS and PMS Li depletion. The early-G (G0–G5) stars in NGC 6475 lie below those of similar colour stars in the Pleiades and mostly above their counterparts in the Hyades. Because NGC 6475 has a metallicity comparable to that of the Hyades, our observations suggest that these stars must have undergone MS Li depletion between

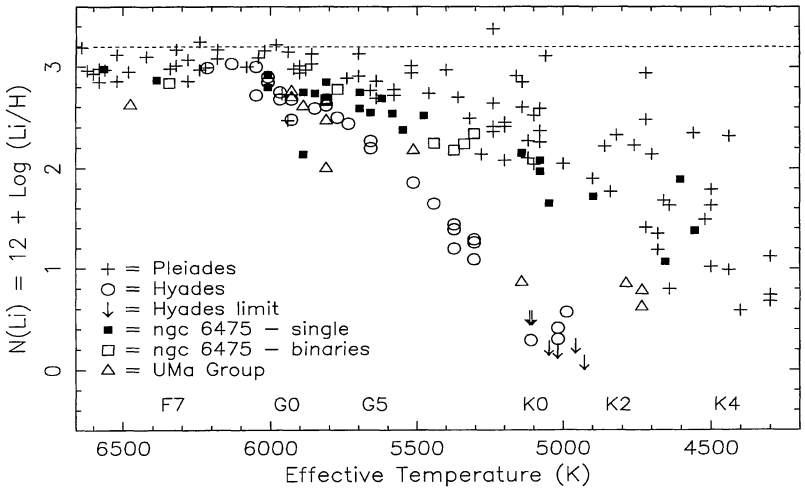

Figure 7. Logarithmic Li I 6708-Å abundances N(Li) = 12 + log(Li/H) versus effective temperature for late-F to K4 stars in the Pleiades, Ursa Major moving Group, Hyades and NGC 6475 are plotted. The dashed line represents the undepleted cosmic Li I abundance of N(Li) = 3.2 (Soderblom et al. 1993b), and approximate spectral types are annotated on the abscissa. Note: the abundance of JJ 1, $T_{\rm eff}$ = 6560 K, has been estimated from data presented in Boesgaard & Tripicco (1986).

220 and 600 Myr and possibly between 70 and 220 Myr, in addition to any PMS depletion they may have experienced. The mid/late-G stars in NGC 6475 exhibit a similar Li depletion pattern to the earlier-G stars, except that more MS depletion must occur *after* the age of NGC 6475 to reproduce the mid/late-G Hyades Li distribution. However, because the K stars in NGC 6475 lie in the lower envelope of Pleiades values, these stars may not have suffered significant MS depletion prior to 220 Myr and yet must undergo a further two orders of magnitude depletion if they are to match the K stars in the Hyades during the next 400 Myr.

At this stage it is worth warning the reader that empirical evidence exists showing a correlation between reduced Li depletion and rapid rotation. The upper envelope of both the Pleiades and α Per Li I EW distribution [$(B-V)_0 \gtrsim 0.60$] is generally populated by the more rapidly rotating cluster members (Soderblom et al. 1993b; Balachandran et al. 1988, 1996). Our sample is X-ray selected and biased towards observations of the most rapidly rotating members in the cluster, therefore if rapid rotation can inhibit Li depletion, it is likely that we have observed the most Li-rich targets in NGC 6475. These objects must still evolve towards the Hyades distribution, but they have probably evolved from stars at the upper envelope of the Pleiades Li distribution. We can conclude that Li I depletion must occur at all masses (late-F to K4) on the MS between 220 and 600 Myr, and probably between 70 and 200 Myr, unless the increased metallicity of NGC 6475 with respect to the Pleiades leads to significantly enhanced PMS depletion.

The Pleiades N(Li) data presented in Fig. 7 shows that there is a definite spread, which grows with decreasing mass, in Li abundance amongst the G and K-dwarfs. However, apart from the early-G stars, there is very little spread in Li abundance amongst the late-type Hyads (Thorburn et al. 1993). Soderblom et al. (1995) have argued that this implies that either PMS depletion leaves the Pleiades – but not the Hyades – with a spread in N(Li) as a result of differing

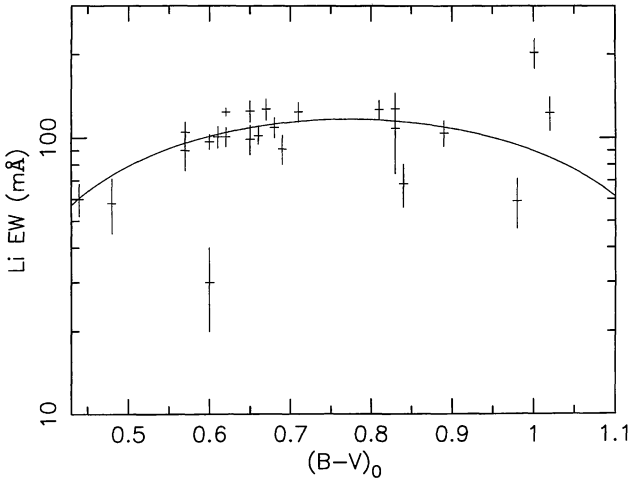

Figure 8. Equivalent width of the Li I 6708-Å doublet line plotted as a function of colour for NGC 6475. The 1σ statistical errors are taken from the Li I data in Table 2. The solid line is a second-order polynomial fit to the data, and indicates little or no scatter for the G (except one extreme point) and early-K stars, and some scatter is evident in the later-K stars, although the fit is poorly constrained in this region of the plot.

metallicity or initial AM distribution, or that some convergence mechanism, perhaps associated with rotation rate, ensures that the Pleiades N(Li) distribution would evolve into that of the Hyades. Following Thorburn et al. (1993), we choose to investigate the dispersion of N(Li) in NGC 6475 in EW/$(B-V)$ space for two reasons. First, ordinate and abscissa error bars are unrelated in the observational plane, whereas in abundance space, $T_{\rm eff}$ errors translate directly to errors in N(Li) determinations. Secondly, curves of growth (COGs) are dependent on varying stellar parameters such as metallicity, surface gravity and microturbulence. Lithium 6708 EWs of single stars in NGC 6475 are plotted as a function of colour in Fig. 8, and the solid line

represents a second-order polynomial fit through all the data aside from the anomalously low point, JJ 4 (discussed below). There is some evidence for scatter in the F, G and early-K stars. The χ^2 summation for these 20 points is 54, suggesting an additional real scatter of about 10 mÅ, corresponding to about ± 0.1 dex in N(Li). This scatter is similar to that observed in the Pleiades and Hyades early-G stars, but might be explained in this case by small errors in the temperature determinations, perhaps as a result of differential reddening. The scatter may increase to an order of magnitude in N(Li) for the mid-K stars (albeit from three points). It is interesting to note that the slowly rotating K star, JJ 20, has a lower Li abundance than the two UFR K stars.

Bearing in mind the rotational selection bias, it is probably not possible to rule out a significant spread of Li abundance in the G and early-K stars, but it appears likely that a spread is present in cooler stars. Unfortunately this means we cannot rule out either of Soderblom et al.'s (1995) suggestions, because the spread is present in stars cooler than those for which Li detections have been reported in the Hyades. If subsequent observations of an unbiased sample were to reveal an unchanged pattern of Li depletion in NGC 6475, this would argue for a PMS origin for the small spread in the Hyades N(Li) distribution. Conversely, if slowly rotating stars had lower Li abundances, particularly around 5000 K, then this might indicate partial convergence of the Li abundances, as a result of some process at work whilst stars were on the MS. At this point it is useful to compare our data with some results for NGC 1039 (age $\sim$200 Myr) presented by Soderblom (1996). His sample has been selected from photometric and proper motion candidates (Soderblom, private communication), and interestingly the data seem to suggest a pattern of Li depletion very similar to that in NGC 6475.

We note that an early-G star (JJ 4) within the cluster has a much lower Li EW (and abundance) in comparison to the remainder of the early-G sample, and lies below the Li abundances of similar stars in the Hyades. The photometry of JJ 4 places it on the cluster MS, and there are four radial velocity measurements of the target, all consistent with membership (Table 2). Furthermore, the target has a cluster-like [Fe/H] value (see Table 4). We must conclude that this target is probably a bona fide low-lithium cluster member, and warrants further observation.

In the Hyades, double-lined spectroscopic binaries exhibit Li abundances defining the upper envelope of N(Li) for a given temperature, or in the case of the two coolest binaries, N(Li) values well above the cluster mean trend (Thorburn et al. 1993). A similar inhibition of Li depletion is observed among RS CVn binaries (Pallavicini, Randich & Giampapa 1992), and may be the result of tidal synchronization of the components, leading to a suppression of mixing and turbulence due to differential rotation (Ryan & Deliyannis 1995). Amongst the spectroscopic binaries in NGC 6475, higher levels of N(Li), compared to the cluster trend, are not observed, although only one SB2 with measurable Li has been observed. There is a grouping of four SBs in the cluster at $T_{\rm eff} \sim 5400$ K and no single stars of similar temperature with which to compare them; however, they appear to lie along a trend linking the mid-G and early-K single stars.

5 COMPARISON OF ROTATION DATA WITH PUBLISHED AML EVOLUTION MODELS

We cannot examine the full rotational distribution of G and K stars in NGC 6475, because our X-ray selected sample is biased towards rapidly rotating cluster members and probably far from complete. Therefore we choose to investigate some diagnostic properties of the most rapidly rotating G and K dwarfs in the cluster, and those in the α Per, Pleiades and Hyades clusters, by comparing their rotation-rate data to rotational evolution model predictions at their respective ages.

The majority of rotation rate measurements for late-type stars are in the form of $v \sin i$ determinations, which is problematic because of the unknown projection angle, i. Measurements of $v \sin i$ for PMS stars can be even less representative of rotation rate because the radius of each star depends upon the precise location of the star on its PMS evolutionary track. To avoid these ambiguities, it is best to investigate the rotational evolution of solar-type stars using rotation periods.

The names, colours and rotational period data of the most rapidly rotating G and K stars known in the α Per, Pleiades, NGC 6475 and Hyades clusters are listed in columns 2–5 of Table 6. The sources of the data are listed in column 6 and we assume these data represent robust estimations of the peak rotation rates in the clusters. It should be noted that there are a couple of more rapidly rotating G stars in the Hyades (e.g. VB 102), although they are G0/1 stars, and it is desirable to have comparison stars with similar colours to the NGC 6475 targets. The reader should further note that the Pleiades G star period is derived from a $v \sin i$ measurement ($v \sin i = 37$ km s^{-1}, Soderblom et al. 1993a), because unfortunately there is no photometric period determination for this star in the literature. How-

Table 6. Targets, colours and rotation period data for the most rapidly rotating G and K stars in the α Per, Pleiades, NGC 6475 and Hyades clusters. Sources of the data are listed in column 6.

Cluster	Target	$(B-V)_0$	P_{rot} (hrs)	Ω_{max} (10^{-5}s^{-1})	Ref
G stars:					
α Per	AP 118	0.71	7.62	22.90	1
Pleiades†	HII 253	0.65	28.23	6.182	2
NGC 6475†	JJ 17	0.69	83.57	2.088	
Hyades	VB 64	0.66	208.08	0.839	3
K stars:					
α Per	AP 100	1.03	4.97	35.12	4
Pleiades	HII 1883	0.99	5.60	31.17	4
NGC 6475‡	JJ 15	1.00	28.75	6.071	
Hyades	VB 175	1.03	259.68	0.672	3

References: 1 – O'Dell & Collier Cameron (1993); 2 – Soderblom et al. (1993a); 3 – Radick et al. (1987); 4 – Prosser et al. (1993). † – Period calculated using $P = 2\pi 0.86\ R_\odot / v \sin i$ (see text). † – Period calculated using $P = 2\pi 0.62\ R_\odot / v \sin i$ (see text).

ever, the true rotation periods of Pleiades stars, both hotter and cooler, indicate that this is a reasonable value. The periods for this star, and the NGC 6475 G and K stars, have been calculated using ZAMS radii determined from mass/radii interpolations of VandenBerg & Bridges (1984), quoted in CC94 as $R_G = 0.86\ R_\odot$ and $R_K = 0.62\ R_\odot$ for G and K stars respectively. The periods for the Pleiades and NGC 6475 G stars, and the NGC 6475 K star, are strictly speaking upper limits, and the true values may be smaller. However, the inferred period of the most rapidly rotating NGC 6475 G star is not likely to be much less than we have estimated because all the G stars observed in the cluster have $L_X/L_{bol} < 10^{-3}$ (see Fig. 3), indicative of equatorial rotation rates $\lesssim 15$ km s^{-1}. The inferred period for the NGC 6475 K star cannot be constrained using the X-ray emission since the target has $v \sin i > 20$ km s^{-1} and $L_X/L_{bol} \sim 10^{-3}$.

5.1 Comparison to the Barnes & Sofia evolution models

The evolutionary tracks of BS96 commence early in the PMS stage while stars are still high up on their Hayashi tracks. They use the Yale Rotating Evolution Code, which includes stellar evolution (e.g. a changing stellar moment of inertia at early times), the effects of AM transport due to a variety of rotationally induced instabilities, and differential rotation between the radiative core and rigidly rotating convective envelope. Models have starting periods (SP) of 4–16 d, matching observed classical T Tauri star periods. An AML saturation angular velocity is introduced (Ω_{sat}, the velocity above which the stellar dynamo is assumed to saturate and the functional form of an AML rate becomes more weakly dependent on velocity), of 10, 8, 5 and 2 $\Omega_\odot$, and AML along the PMS and MS is simulated with a Kawaler-like (Kawaler 1988) AML prescription (wind geometry index, $N = 1.5$ and stellar magnetic field strength scaling linearly with rotation, i.e. $B \propto \Omega$) until the models reach the solar radius, luminosity and rotation rate.

None of the solar mass models presented in BS96 are able to *simultaneously* fit the angular velocities of the most rapidly rotating G stars in the α Per, Pleiades and NGC 6475 clusters. A model which fits the first two clusters is rotating too slowly by the age of NGC 6475 compared to the observationally measured value. Moreover, we can interpolate between the 0.8- and 0.6-$M_\odot$ models of BS96 to compare with our K star ($\sim 0.7\ M_\odot$) data. Again, it appears that the lower mass models of BS96 cannot *simultaneously* fit the rapid rotator data of all three clusters. The discrepancy is in the same sense as for the G stars, although smaller. A few plausible hypotheses can be put forward which might explain the current discrepancies between a single BS96 model and the full multi-cluster data set.

(i) The ages of the Pleiades or NGC 6475 are incorrect. The models and data would be more compatible if the Pleiades were systematically older or NGC 6475 younger. The age of the Pleiades, derived by Mermilliod (1981), is 78 Myr although many authors choose to quote a value of 70 Myr. Furthermore, Meynet et al. (1993) derive an age of $\sim$100 Myr for the age of the Pleiades (with the same MS isochrones used to derive the age of NGC 6475), which has significant implications for both the G and K star evolutionary models (see above). Basri, Marcy & Graham (1996) also report an older age estimate of the Pleiades, based upon lithium detections in Pleiades brown dwarf candidates.

(ii) Surface magnetic field configurations become more closed as the stars evolve from the Pleiades to NGC 6475. Assuming the cluster ages are correct, the observations indicate that the AML rate of G and K Pleiads becomes *smaller* than the BS96 adaptation of the Kawaler AML prescription predicts, as the stars evolve along the MS to the age of NGC 6475. The rate of AML is a function of the geometry of the dynamo-induced surface magnetic field (wind index N, Kawaler 1988). If the B-field configuration becomes more closed and complex, then decreasing N reduces the AML in stars between the Pleiades and NGC 6475, the gradients of the evolutionary tracks become more shallow, and a scenario could be constructed in which a single model fits the data. However, it seems more plausible for the magnetic field to become more closed as the rotation speed *increases*, because it is from regions of closed magnetic field that the coronal X-ray emission arises.

(iii) The ad hoc hypothesis that all open clusters are not alike and exhibit varying physical characteristics beyond those expected from a coeval group of stars of given age and composition. If we assume that the initial angular velocities of PMS NGC 6475 members were significantly greater than those of their Pleiades counterparts, then observed angular velocities of NGC 6475 stars would be higher compared to an evolutionary track fitting the Pleiades rotation rates. We draw the readers' attention to the preliminary results on NGC 1039, presented by Soderblom (1996). This cluster has an age of 200 Myr, but appears to have some G stars rotating at 20 km s^{-1} and K stars at 30–40 km s^{-1}. It may be that a careful comparison of NGC 6475 and NGC 1039 would reveal true cluster-to-cluster variations at the same age.

(iv) A solution involving centrifugal driving. This mechanism causes additional acceleration of the plasma in a stellar wind as a result of a centrifugal force, and forces the plasma to rotationally decouple from the stellar magnetic field at a smaller distance from the star, reducing the AML flux lost as a result of the wind (see equations 1 and 8, CC94). This reduction in AML efficiency arising from centrifugal driving may be compensated for by increasing the AML saturation velocity. The net effect could provide an initial steep drop in rotation rates between α Per and the Pleiades, but a shallower descent to ages of 220 Myr (see next section).

If we accept the BS96 models as a correct physical description for the spin-down of late-type stars and address the observed discrepancy by assuming a Pleiades age of 100 Myr, then some interesting results are obtained.

A BS96 1-$M_\odot$ evolutionary track with SP = 4 d (the assumed value for the fastest rotating stars on the birth line) and $\Omega_{sat} = 8\ \Omega_\odot$ successfully fits the α Per and Pleiades points, but does not fit NGC 6475. The predicted rotation rate at 220 Myr is too slow to match the observational data. A better solution would be to have SP $\sim$ 6 d and $\Omega_{sat} \sim 6\ \Omega_\odot$. A slightly longer SP is probably justified, because the observed T Tauri stars from which the SPs were obtained have evolved some way from the stellar birth line used as the initial point by BS96, and have presumably contracted and spun-up to some degree. For 0.7-$M_\odot$ stars, it is likely that an

SP = 4 d, $\Omega_{sat} \simeq 3\ \Omega_\odot$ model will successfully fit all the data if the Pleiades age is allowed to increase to 100 Myr.

The best-fitting BS96 models indicate that the dynamo saturation velocity required to fit the rotation rate data of solar mass stars in young open clusters is about twice the magnitude of that required for the K stars, and suggests that the dynamo saturation velocity is *mass dependent*. Noyes et al. (1984) demonstrated that the apparent mass-dependency of chromospheric emission in late-type field stars was less evident when the data were plotted against R_o instead of rotation rate. We have calculated R_o for each best-fitting Ω_{sat} in the G and K star BS96 evolutionary tracks (assuming $\Omega_{sat} = 6\ \Omega_\odot$, $P_{sat} \simeq 4$ d for G stars and $\Omega_{sat} = 3\ \Omega_\odot$, $P_{sat} \simeq 8$ d for K stars). Convective turnover times have been calculated using the colour–τ_c relation in Rucinski & Vandenberg (1990),[2] and we find $\tau_c(G) = 10.0$ d and $\tau_c(K) = 21.3$ d. Therefore, a single saturation Rossby number of about 0.4 can account for the rapidly rotating G *and* K stars in a single cluster. However, if we translate these saturation velocities into equatorial velocities then $V_{eq} \simeq 12$ and 6 km s^{-1} for G and K stars, respectively. It may be difficult to reconcile these dynamo saturation rotation rates with observations of saturated X-ray emission above $v \sin i = 15$–20 km s^{-1} in a number of open clusters (e.g. Stauffer et al. 1994). Two mechanisms for increasing the AML saturation velocity are reduced interior AM transport, perhaps arising from the coupling of the core and envelope with poloidal magnetic fields (Charbonneau & MacGregor 1993), or centrifugal driving of the stellar wind at high rotation speeds. Both of these effects are simulated in the solid-body AML models presented by CC94.

5.2 Comparison with the CC94 evolution models

The evolutionary tracks of CC94 use a parametrization of the Weber & Davis (1967) solid-body stellar wind model, with a linearly rotation-scaled dynamo relation, and include the effects of AML saturation, and a thermo-centrifugal wind driving model. The models commence at 30 Myr (neglecting evolutionary changes in the stellar radius, and hence moment of inertia) with ZAMS break-up velocities ($\Omega_0 = [GM_*/4R_*^3]^{1/2}$) and evolve along the MS to produce reasonable fits to both the fastest rotators in the Pleiades and the present-day solar rotation rate (for G stars). The main difference between the CC94 AML prescription and that of a Kawaler-like model is the weakening of the rotation rate dependence of the braking rate as a result of centrifugal driving.

The best-fitting CC94 solar mass model is able to simultaneously fit the angular velocities of the most rapidly rotating G stars in the α Per, Pleiades (with age = 80 Myr), NGC 6475 and Hyades clusters. The saturation velocity of the best-fitting 1-M$_\odot$ model is $\sim 28\ \Omega_\odot$, indicating that solid-body rotation and centrifugal driving serve to raise the value of the saturation velocity. Furthermore, this saturation velocity translates into an equatorial velocity $\simeq 56$ km s^{-1}, which is far higher than that inferred from observations of saturated X-ray emission of solar-type stars.

[2]Note: the Rucinski & Vandenberg colour–τ_c relation does not extend past $B - V \sim 0.95$, although we use their relation to calculate the value of τ_c for the K stars.

For lower mass stars, the CC94 models are less successful. A best-fitting 0.7-M$_\odot$ model which simultaneously fits the angular velocities of the most rapidly rotating K stars in the α Per, Pleiades and Hyades clusters *cannot* fit the NGC 6475 point, with a velocity prediction ($V_{eq} \simeq 5$ km s^{-1}) at 220 Myr which is half an order of magnitude below the spectroscopically measured lower limit. In order to provide a simultaneous fit to the data of all four clusters, the gradient of the rotational evolution must become more shallow during the first 150 Myr. There are two probable causes for the discrepancy between CC94's K star models and the observational data. First, mid-K stars do not arrive on the main sequence until ~ 70 Myr (Pinsonneault, Kawaler & DeMarque 1990), therefore at 30 Myr a mid-K star is still contracting along its PMS track and spinning-up (or at least partially counteracting any AML it experiences). This causes the magnitude of $d\Omega/dt$ to decrease. Secondly, the boundary condition of a K star having a break-up rotational velocity at 30 Myr is unrealistic because it is likely these stars will continue to spin-up because of gravitational contraction at this epoch, and therefore none will survive to the ZAMS because they will have broken up. We also note that this model deficiency is also of concern (albeit to a lesser extent) for solar mass stars because they are expected to arrive on the main sequence at an age of ~ 40 Myr (Pinsonneault et al. 1990).

We can also compare our G star rapid rotator data to the solar mass evolutionary tracks presented in Bouvier (1994). The models commence with an SP of 8 d and are subject to AML using a solid-body Kawaler-like braking law with dynamo/AML saturation occurring above 60 km s^{-1}. A linear dynamo is used below this velocity and $B \propto \Omega^{1/2}$ above it. Rotational evolution in their models is further constrained by coupling between an accretion disc and the stellar magnetic field, during the PMS phase, for a series of different disc lifetimes (model rotation periods remain constant while disc-star coupling is occurring because of the underlying assumption that disc-star coupling, PMS spin-up due to contraction and spin-down due to AML are in equilibrium). Again, the models cannot simultaneously fit the rapid rotator data for solar mass stars in the α Per, Pleiades, NGC 6475 and Hyades clusters. In addition, their tracks cannot fit the most rapidly rotating G star in α Per, no matter how early a star is permitted to decouple from its accretion disc. Furthermore, by the age of the Hyades, the majority of the evolution tracks of the Bouvier models have converged and predict rotational velocities *below* the equatorial velocities of Hyads with photometrically determined periods.

We conclude that CC94's solid-body models, which include centrifugal driving, can simultaneously fit the G star rapid rotator data in the α Per, Pleiades, NGC 6475 and Hyades clusters, but their K star models, the solid-body solar mass models of Bouvier (1994), and the differentially rotating BS96 G and K star models are *unable* to simultaneously match the rapid rotator data in these clusters. A plausible increase of the Pleiades age to 100 Myr makes a BS96 solution possible. The main effect of including AM transport is to reduce the value of Ω_{sat} required. The best-fitting BS96 models indicate that the required saturation velocity is mass dependent, although a model with a single saturation Rossby number of ~ 0.4 can simultaneously account for the

rapidly rotating G and K stars in young open clusters. Both CC94 and BS96 models which simultaneously fit the cluster data predict saturation velocities which are inconsistent with the value inferred from observations of saturated coronal emission. The solid-body models of BS96 yield saturation velocities below those inferred from observations of saturated X-ray emission, which is difficult to explain. The inclusion of centrifugal driving and a solid-body rotation assumption in AML models yields Ω_{sat} values much higher than obtained for the differentially rotating models and a factor of 3–4 greater than those inferred from observations of saturated X-ray emission. These facts may be consistent if coronal saturation is not indicative of true saturation of the large-scale magnetic field strength (see O'Dell et al. 1995). It is likely that the inclusion of more realistic boundary conditions and evolutionary changes in the stellar moment of inertia at early times will reduce the Ω_{sat} required in CC94's models and possibly provide reasonable fits to the K star rapid rotator data as well.

6 SUMMARY

An X-ray selected sample of optical counterparts to the *ROSAT* PSPC detections in the 220 Myr open cluster NGC 6475 has been observed for radial and rotational velocities, chromospheric activity and lithium abundances. NGC 6475 is the closest and most compact open cluster of those that occupy the astrophysically important position midway in age between the nearby and well-studied Pleiades and Hyades clusters and is at a diagnostically important age for the investigation of proposed mechanisms of AML in late-type stars and the depletion of lithium in their convective envelopes. Based on the available photometry and measured radial velocities, we have found 26 probable single cluster members, nine probable cluster binaries and eight possible cluster binaries. Our sample is X-ray selected, and should include the most rapidly rotating G and K stars in the cluster, but is unlikely to be complete for the slowest rotators. Comparison of the spectroscopic data to synthetic spectra has allowed us to calculate $[\mathrm{Fe/H}] = +0.110 \pm 0.034$ for the cluster, and has revealed possible evidence for differential reddening. The metallicity of the cluster is comparable to that of the Hyades, but may be different enough from the Pleiades to make a difference to patterns of Li depletion.

We have detected NGC 6475 G stars with $v \sin i$ between ≤ 6 and ~ 13 km s^{-1}, indicating that the most rapid G stars in the cluster are still rotating faster than their slowest counterparts in the α Per, Pleiades and Hyades clusters. The $v \sin i$ distribution of early-K stars in NGC 6475 is in the range ≤ 6–10 km s^{-1}, and assuming we have observed the most rapidly rotating stars in the cluster, the G and early-K $v \sin i$ data are indicative of significant, but not complete, spin-down and convergence after ~ 150 Myr on the MS. The degree of spin-down is less for the mid-K dwarfs, where we detect two rapid rotators with $v \sin i$ in excess of 20 km s^{-1} and with $L_X/L_{bol} \sim 10^{-3}$. Taken together with observations of other open clusters, these results argue for mass-dependent e-folding spin-down time-scales ranging from about 20 Myr for early-G stars to > 75 Myr for mid-K stars.

Coronal activity in NGC 6475 appears well correlated with rotation in the sense that all G and early-K stars in the cluster have $L_X/L_{bol} < 10^{-3}$, indicative of rotation rates ≤ 15 km s^{-1}, in agreement with their measured $v \sin i$. Furthermore, two mid-K dwarfs exhibit saturated levels of X-ray emission and $v \sin i > 20$ km s^{-1}, consistent with the current rotation–coronal activity paradigm of saturation in late-type stars. For the majority of our sample, levels of chromospheric activity in the cluster lie just below the lower envelope of the Pleiades activity distribution, and maximum (possibly saturated) levels of activity in NGC 6475 are reached in lower mass stars than in the Pleiades. A possible saturation in Hα and Ca II 8542-Å flux exists for $v \sin i \gtrsim 15$ km s^{-1} in late-type Pleiads (S93), and our results show that $L_{H\alpha}/L_{bol}$ and L_{8542}/L_{bol} reach maximum values of $\sim 10^{-4}$ and $10^{-4.2}$ respectively, comparable with the saturation-like levels observed in the Pleiades. We have also shown that there is a general correlation of coronal versus chromospheric activity in the cluster.

Observations of the Li I 6708-Å line for late-F to K4 stars in NGC 6475 show that MS Li depletion must occur between the ages of NGC 6475 and the Hyades and probably between the Pleiades and NGC 6475, although the metallicity difference between the Pleiades and NGC 6475 may lead to differences in PMS Li depletion which could explain the observed abundances. The large scatter observed in Pleiades K star Li abundances is not prominent in NGC 6475, although the three mid-K stars have Li abundances inconsistent with a single valued Li abundance–mass relationship. The G and early-K stars in NGC 6475 show some evidence for a small scatter about such a relationship, although the possibility of differential reddening and the bias against the observation of slow rotators in our sample, combined with empirical evidence relating inhibited Li depletion and rapid rotation, make this conclusion tentative. Unfortunately, we cannot therefore discriminate between a PMS origin for the difference in Li abundance scatter in the Pleiades and Hyades G and K stars or a convergence mechanism operating on the MS which would evolve the Pleiades Li abundances into those seen in the Hyades. Higher levels of Li abundance are not observed in the probable spectroscopic binaries of NGC 6475.

We have compared our rotation data for the most rapidly rotating G and K stars in NGC 6475 to published sets of rotational evolution models. These models are used to describe the rotation rates of the most rapidly rotating stars in the α Per, Pleiades, NGC 6475 and Hyades clusters. The major finding (in common with other authors who have constructed similar AML models, e.g. Krishnamurthi et al. 1997) is that models incorporating differential rotation (BS96) are unable to simultaneously fit the rapidly rotating stars of all four clusters. Several hypotheses are presented which may explain the discrepancy between the models and observations. The most likely are that the age of the Pleiades could be increased to 100 Myr, that centrifugal wind driving at high rotation rates should be included or that there might simply be differences in the initial AM distributions in individual clusters.

Assuming an increase in the Pleiades age, the BS96 models require a saturation velocity which is mass dependent. Both the G and K stars can be modelled if a single saturation Rossby number of ~ 0.4 is used. This value

implies dynamo saturation rotation rates of 12 km s^{-1} and 6 km s^{-1} for G and K stars, respectively, which may be too low to be compatible with observations of saturated X-ray emission. Saturation can be moved to higher rotation rates if the rate of interior AM transport is reduced or if centrifugal wind driving becomes important. The effects of centrifugal driving are included in the solid-body rotational evolution models presented in CC94. Although their initial boundary conditions are unrealistic and the evolution of the moment of inertia at early times has been ignored, their best-fitting solar mass models can simultaneously fit the G star rapid rotator data in these clusters, with a saturation velocity of $\sim 28\ \Omega_{\odot}$. Their K star models cannot simultaneously fit the rotation data for the α Per, Pleiades, NGC 6475 and Hyades clusters. These problems might be resolved if realistic boundary conditions and an evolving moment of inertia are used.

Two lines of attack are suggested by this current work, in order to more fully evaluate the properties of NGC 6475. The sheer density of stars in the field is a major problem in identifying cluster members. One solution is to observe the cluster with the high resolution imager on board the *ROSAT* satellite. This will give much smaller (2–3 arcsec) error circles enabling firm identification of optical counterparts. This does not help with the second main problem, which is overcoming the bias inherent in an X-ray selected sample of cluster members. We plan to obtain radial velocities for large numbers of photometrically selected candidates with fibre spectrographs in order to obtain an optically selected sample. Only then will it be possible to study the true rotation and lithium abundance distribution among the G and K stars and to extend our studies to lower masses. A comparison of the rapid rotator data for young open cluster G and K stars to models similar to those of CC94, but which include the effects of stellar moment of inertia evolution and a more realistic set of boundary conditions, is planned.

ACKNOWLEDGMENTS

We thank the Directors and staff of the Anglo-Australian Observatory, Mount Stromlo Observatory and South African Astronomical Observatory and the Particle Physics and Astronomy Research Council (PPARC) for travel and subsistence grants. It is a pleasure to acknowledge Charles Prosser for useful discussions and his provision of unpublished photometric data, and other data prior to publication. We also thank Professor Gordon Bromage for his assistance in collecting the SAAO data, and Dr Barry Smalley for his assistance with the UCLSYN software. DJJ acknowledges the financial support of the Astrophysics and Space Research group at the University of Birmingham and Mrs J. Pryer. Computational work was performed on the Birmingham and Keele nodes of the PPARC-funded Starlink network. This research has made use of the Simbad data base, operated at CDS, Strasbourg, France, and NASA's Astrophysics Data System Abstract Service. Finally, we thank the anonymous referee for helpful comments on the initial draft of this paper.

REFERENCES

Abt H. A., Levy S. G., Baylor L. A., Hayward R. R., Jewsbury C. P., Snell C. M., 1970, ApJ, 159, 919
Allan D. J., 1992, Starlink User Note 4, Rutherford Appleton Laboratory
Balachandran S., Lambert D. L., Stauffer J. R., 1988, ApJ, 333, 267
Balachandran S., Lambert D. L., Stauffer J. R., 1996, ApJ, 470, 1243
Barnes S., Sofia S., 1996, ApJ, 462, 746 (BS96)
Basri G., Marcy G. W., Graham J. R., 1996, ApJ, 458, 600
Bessell M., 1979, PASP, 91, 589
Boesgaard A. M., Friel E. D., 1990, ApJ, 351, 467
Boesgaard A. M., Tripicco M. J., 1986, ApJ, 303, 724
Bohlin R. C., Savage B. D., Drake J. F., 1978, ApJ, 224, 132
Bouvier J., 1994, in Caillault J.-P., ed., ASP Conf. Ser. Vol. 64, 8th Cambridge Workshop on Cool Stars, Stellar Systems and the Sun. Astron. Soc. Pac., San Francisco, p. 151
Breger M., 1986, ApJ, 309, 311
Briel U. G., Pfeffermann E., 1986, Nucl. Instrum. Methods Phys. Res., 242, 376
Chaboyer B., DeMarque P., Pinsonneault M. H., 1995, ApJ, 441, 876
Charbonneau P., MacGregor K. B., 1993, ApJ, 417, 762
Collier Cameron A., Li J., 1994, MNRAS, 269, 1099 (CC94)
Collier Cameron A., Campbell C. G., Quaintrell H., 1995, A&A, 298, 133
D'Antona F., Mazzitelli I., 1984, A&A, 138, 431
Endal A. S., Sofia S., 1981, ApJ, 243, 625
Favata F., Micela G., Sciortino S., 1996, A&A, 311, 951
Foing B. H., Crivellari L., Vladilo G., Rebolo R., Beckman J. E., 1989, A&AS, 80, 189
Friel E. D., Boesgaard A. M., 1992, ApJ, 387, 170
Gieseking F., 1985, A&AS, 61, 75
Gray D. F., 1992, The Observation and Analysis of Stellar Photospheres, 2nd edn. Cambridge Univ. Press, Cambridge
Hempelmann A., Schmitt J. H. M. M., Schultz M., Rüdiger G., Stępien K., 1995, A&A, 294, 515
Jeffries R. D., Thurston M. R., Pye J. P., 1997, MNRAS, 287, 350
Johnson H., 1966, ARA&A, 4, 193
Kawaler S. D., 1988, ApJ, 333, 236
Koelbloed D., 1959, Bull. Astron. Inst. Netherlands, 14, 265
Kraft R. P., 1967, ApJ, 150, 551
Krishnamurthi A., Pinsonneault M. H., Barnes S., Sofia S., 1997, ApJ, 480, 303
Kürster M., Schmitt J. H. M. M., 1996, A&A, 311, 211
Kurucz R. L., 1991, in Davis Philip A. G., Upgren A. R., Janes K. A., eds, Precision Photometry: Astrophysics of the Galaxy. Davis Press, Schenectady, p. 27
Kurucz R. L., Bell B., 1995, Smithson. Astrophys. Obs., Tech. Rep.
Lang K. R., 1991, Astrophysical Data – Planets and Stars. Springer-Verlag, New York
Li J., Collier Cameron A., 1993, MNRAS, 261, 766
Linsky J. L., Hunten D. M., Sowell R., Glackin D. L., Kelch W. L., 1979, ApJS, 41, 481
MacGregor K. B., Charbonneau P., 1994, in Caillault J.-P., ed., ASP Conf. Ser. Vol. 64, 8th Cambridge Workshop on Cool Stars, Stellar Systems and the Sun. Astron. Soc. Pac., San Francisco, p. 174
Menzies J. W., Marang F., 1996, MNRAS, 282, 313
Mermilliod J.-C., 1981, A&A, 97, 235
Meynet G., Mermilliod J.-C., Maeder A., 1993, A&AS, 98, 477
Mills D., Webb J., 1994, Starlink User Note 152, Rutherford Appleton Laboratory

Noyes R. W., Hartmann L. W., Baliunas S. L., Duncan D. K., Vaughan A. H., 1984, ApJ, 279, 763
O'Dell M. A., Collier Cameron A., 1993, MNRAS, 262, 521
O'Dell M. A., Panagi P., Hendry M. A., Collier Cameron A., 1995, A&A, 294, 715
Pallavicini R., Randich S., Giampapa M. S., 1992, A&A, 253, 185
Peterson R., 1985, ApJ, 294, L35
Pinsonneault M. H., 1994, in Caillault J.-P., ed., ASP Conf. Ser. Vol. 64, 8th Cambridge Workshop on Cool Stars, Stellar Systems and the Sun. Astron. Soc. Pac., San Francisco, p. 255
Pinsonneault M. H., Kawaler S. D., DeMarque P., 1990, ApJS, 74, 501
Pinsonneault M. H., Deliyannis C., DeMarque P., 1991, ApJ, 367, 239
Proffitt C. R., Michaud G., 1989, ApJ, 346, 976
Prosser C. F., 1992, AJ, 103, 488
Prosser C. F. et al., 1993, PASP, 105, 1407
Prosser C. F., Stauffer J. R., Caillault J.-P., Balachandran S., Stern R. A., Randich S., 1995, AJ, 110, 1229 (P95)
Prosser C. F., Randich S., Stauffer J. R., 1996, AJ, 112, 649
Radick R. R., Thompson D. T., Lockwood G. W., Duncan D. K., Baggett W. E., 1987, ApJ, 321, 459
Robinson R. D., Carpenter K. G., Slee O. B., Nelson G. J., Stewart R. T., 1994, MNRAS, 267, 918
Rucinski S. M., Vandenberg D. A., 1990, AJ, 99, 1279
Rutten R. G. M., 1987, PhD thesis, Univ. Utrecht
Ryan S. G., Deliyannis C. P., 1995, ApJ, 453, 819
Schatzmann E., 1962, Ann. Astrophys., 25, 18
Schmitt J. H. M. M., Micela G., Sciortino S., Vaiana G. S., Harnden F. R., Jr, Rosner R., 1990, ApJ, 351, 492
Skumanich A., 1972, ApJ, 171, 565
Smith K. C., 1992, PhD thesis, Univ. London
Snowden M. S., 1976, PASP, 88, 171
Soderblom D. R., 1996, in Pallavicini R., Dupree A. K., eds, ASP Conf. Ser. Vol. 109, 9th Cambridge Workshop on Cool Stars, Stellar Systems and the Sun. Astron. Soc. Pac., San Francisco, p. 315
Soderblom D. R., Mayor M., 1993, AJ, 105, 226
Soderblom D. R., Oey M. S., Johnson D. R. H., Stone R. P. S., 1990, AJ, 99, 595
Soderblom D. R., Stauffer J. R., Hudon J. D., Jones B. F., 1993a, ApJS, 85, 315 (S93)
Soderblom D. R., Jones B. F., Balachandran S., Stauffer J. R., Duncan D. K., Fedele S. B., Hudon J. D., 1993b, AJ, 106, 1059
Soderblom D. R., Pilachowski C. A., Fedele S. B., Jones B. F., 1993c, AJ, 105, 2299
Soderblom D. R., Jones B. F., Stauffer J. R., Chaboyer B., 1995, AJ, 110, 729
Spencer-Jones J. H., 1980, Mon. Notes Astron. Soc. S. Afr., 39, 89
Stauffer J. R., 1991, in Catalano S., Stauffer J. R., eds, NATO ASI Series: Angular Momentum Evolution of Young Stars. Kluwer, Dordrecht, p. 117
Stauffer J. R., Hartmann L. W., 1987, ApJ, 318, 337
Stauffer J. R., Hartmann L. W., Latham D., 1987, ApJ, 320, L51
Stauffer J. R., Hartmann L. W., Jones B. F., 1989, ApJ, 346, 160
Stauffer J. R., Caillault J. P., Gagné M., Prosser C. F., Hartmann L. W., 1994, ApJS, 91, 625
Stauffer J. R., Hartmann L. W., Prosser C. F., Randich S., Balachandran S., Patten B. M., Simon T., Giampapa M. S., 1997, ApJ, 479, 776
Stern R. A., Schmitt J. H. M. M., Rosso C., Pye J. P., Hodgkin S. T., Stauffer J. R., 1992, ApJ, 399, L159
Stern R. A., Schmitt J. H. M. M., Pye J. P., Hodgkin S. T., Stauffer J. R., Simon T., 1994, 427, 808
Swenson F. J., Stringfellow G. S., Faulkner J., 1990, ApJ, 348, L33
Thorburn J. A., Hobbs L. M., Deliyannis P., Pinsonneault M. H., 1993, ApJ, 415, 150
Tonry J. L., Davis M., 1979, AJ, 84, 1511
VandenBerg D. A., Bridges T. J., 1984, ApJ, 278, 679
Vilhu O., 1984, A&A, 133, 117
Walker D. D., Diego F., 1985, MNRAS, 217, 355
Weber E. J., Davis L. D., Jr, 1967, ApJ, 148, 217
Wilson O. C., 1963, ApJ, 138, 832
Wilson O. C., 1966, ApJ, 144, 695
Zombeck M. V., 1990, Handbook of Space Astronomy and Astrophysics, 2nd edn. Cambridge Univ. Press, Cambridge